REPROCESSING SILICON CARBIDE INERT MATRIX FUELS BY USING A MOLTEN SALT REACTION/DISSOLUTION METHOD

By

TING CHENG

A DISSERTATION PRESENTED TO THE GRADUATE SCHOOL
OF THE UNIVERSITY OF FLORIDA IN PARTIAL FULFILLMENT
OF THE REQUIREMENTS FOR THE DEGREE OF
DOCTOR OF PHILOSOPHY

UNIVERSITY OF FLORIDA

2010

To my beloved families and friends

ACKNOWLEDGMENTS

My sincerest acknowledgement goes to Dr. Ronald Baney for his wise guidance and unconditional support. He taught me to think not only from an engineering perspective but also in a scientific and fundamental way. His encouragement made me to continuously develop my potential. I'd also like to thank Dr. Charles Beatty for his believe in my ability. Without them, my life path would become totally different from now. I also thank Professor Tulenko for his help on my research and career and for leading me into the nuclear industry. My sincere acknowledgement also goes to my committee members Dr. Jones, Dr. Mecholsky and Dr. Sigmund for their comments on my research and generosity on equipment usage.

I'd like to thank all of the current and former members of Dr. Baney's group: Liwen Jin, Edward McKenna, Ravi Kumar Vasudevan, Chunghao Shih and Le Song for their kind help, both personal and academic. Edward Mckenna and Aniket Selarka deserve special thanks since they were always available to discuss questions and bring about constructive suggestions. I'd also like to thank Soraya Benitez, a former postdoctor in Dr. Baney's group, who proposed the molten salt reaction method to reprocess SiC IMFs. I gratefully thank Department of Energy (DOE) for financially support my doctoral project.

Finally, my deepest gratitude goes to my beloved families, who always support me with their unlimited affection and my fiancé, who is always there for me without any complain. Without their love and encouragement, I would never have come this far. This dissertation is affectionately dedicated to them.

TABLE OF CONTENTS

Page

LIST OF TABLES

LIST OF FIGURES

LIST OF ABBREVIATIONS

AHPCS	Allyl-hydrido-poly-carbo-silane
CVD	Chemical vapor deposition
DS	Directing sintering
EDS	Energy dispersive spectrometry
HP-SiC	Hot-pressed silicon carbide
ICP	Inductive coupled plasma
IM	Inert matrix
IMF	Inert matrix fuel
LPS	Liquid phase sintering
LWR	Light water reactor
MA	Minor actinides
MOX	Mixed oxide
PIP	Polymer infiltration processing
PPP	Pre-ceramic polymer precursor
RB-SiC	Reaction-bonded silicon carbide
SEM	Scanning electron microscopy
TEM	Transmission electron microscopy
XRD	X-ray diffraction
YAG	Yttrium-aluminum-garnet

Abstract of Dissertation Presented to the Graduate School
of the University of Florida in Partial Fulfillment of the
Requirements for the Degree of Doctor of Philosophy

REPROCESSING SILICON CARBIDE INERT MATRIX FUEL BY USING A MOLTEN SALT REACTION/DISSOLUTION METHOD

By

Ting Cheng

December 2010

Chair: Ronald Baney
Major: Materials Science and Engineering

Silicon carbide is one of the prime candidates as a matrix material in inert matrix fuels (IMF) designed to reduce the plutonium stockpiles and minor actinides. It is necessary to separate the non-transmuted actinides and non-fissioned plutonium from the silicon carbide matrix for recycling because complete fission and transmutation is not practical in a single in-core run. In this work, a reaction/dissolution approach to reprocess silicon carbide (SiC) IMFs was proposed. SiC reacts with the molten sodium carbonate (Na_2CO_3) and potassium carbonate (K_2CO_3), to form water soluble sodium or potassium silicate which can be dissolved rapidly in hot water. The optimal processing conditions for reprocessing the SiC IMFs were recommended based on the studies on the salt type, salt depth, atmospheres, partial pressure of the oxidizing gases, total gas flow rate and reaction time. The SiC reaction rate in the molten salts was increased by reducing the molten salt depth, which is a distance between the salt/gas interface to the upper surface of SiC pellets. The K_2CO_3 salt is more effective at 1050 ºC compared to Na_2CO_3, when the initial molten salt depths were kept constant for both salts.

This reprocessing method was further developed through comparison of the reaction rates in air, O_2/Ar, CO_2/Ar, H_2O/Ar, H_2O/CO_2 and H_2O/O_2 with different partial

pressure. The rate was increased by increasing the partial pressure of the reactive gases. Water vapor was firstly introduced in the SiC/K_2CO_3 system. The SiC reaction rate in the H_2O atmosphere was dramatically enhanced 3-4 fold compared to the rate under the O_2 atmosphere. The rate was increased with an increase in the partial pressure of H_2O and the reaction time. Ceria (CeO_2), a surrogate for plutonium oxide (PuO_2), was found intact in these molten salt environments under different atmospheres. Separation of ceria was achieved by dissolving the SiC corrosion product in hot water. The hypothesis that diffusion of the oxidizing gases in the salt is the controlling factor of the SiC/salt reaction at 1050 ºC was proposed and verified in this research.

CHAPTER 1
INTRODUCTION

1.1 Statement of Problem and Motivation

The surplus of plutonium from dissembled nuclear weapons and spent nuclear fuels is considered to be a potential hazard related to proliferation and environmental safety. Approximately 200 tones weapon grade plutonium and 1000 tones civilian plutonium has been produced at the end of the last century. [1] Besides Pu, disposal of minor actinides such as americium (Am), neptunium (Np) and curium (Cm) produced by reprocessing of the spent nuclear fuels is also a major concern because those minor actinides have extremely long half-life. [2]

United States planned to dispose the spent fuels geologically without reprocessing Pu. [1] This strategy requires the storage facilities to be irradiation tolerant for thousands of years. In other countries such as United Kingdom and France, Pu is transmuted into fission products with short half life (less than 30 years) in the form of MOX (mixed oxide of uranium and plutonium) in the light water reactors (LWRs) before geological storage. [1, 3-5] However, this method may result in a larger proliferation risk, because new plutonium and minor actinides are produced in reactors by neutron capture of U^{238} oxide. [1, 3-5] Since MOX fuel does not efficiently reduce Pu stockpiles, inert matrix (IM) materials have been developed recently as a replacement of uranium oxide. The inert matrix is designed to contain less or no fertile materials and not to generate additional actinides wastes or fissile isotopes.

According to the original definition of IM materials, elements of such material should be transparent to neutrons. Potential IM candidates need to possess the following properties as well: high melting point, good thermal conductivity, compatibility

with cladding and coolant, good irradiation stability, mechanical stability during irradiation and good leaching properties if designed for reprocessing and multi-recycling. [1] Most studied inert matrix materials are categorized into metal based oxides, carbides and nitrides (e.g. MgO, ZrC and TiN) and silicon based carbides and nitrides (e.g. SiC and Si_3N_4). [1]

Since it is impractical to achieve complete burnup of Pu and minor actinides during an in-core cycle, developing the techniques for separating the non-transmuted fuel from the inert matrix becomes necessary in order to fabricate them into new fuel elements for repeated burning cycles. [3] Metal oxide based inert matrix materials were reported to dissolve in nitric acid, which is compatible to the traditional reprocessing approach. [3] Metal nitride and carbide can be separated through chlorination and electrochemical etching at 400 ºC. [6]

Silicon carbide (SiC) is one of the prime IMF materials for burning plutonium and long-lived actinides, sine this material holds excellent neutronic and thermal performance capabilities. [7] A significant amount of research supports silicon carbide as a suitable matrix for reprocessing spent fuels. [7-8] However, little attention has been given to identify the techniques for reprocessing and separating transuranic species and unspent fuel from the SiC inert matrix. This research focuses on filling the gap in knowledge by investigating possible techniques for separating a surrogate material for plutonium from silicon carbide.

1.2 Scientific Approach

Efficient techniques for processing and separating transuranic species and unburned fuel from a silicon carbide matrix have not been identified, which hinders its

application as an inert matrix. Potential strategies [6] have been proposed to separate the untransmuted fuel from the inert matrix:

1. Dissolve the matrix but keep fuel as a solid, and then to separate them by filtration;
2. Dissolve the nuclear fuel not the matrix, and then to separate them by filtration;
3. Dissolve both and use a chemical approach to separate them;
4. Volatilize the inert matrix;
5. Volatilize the fuel compounds.

A literature survey was performed to evaluate possible methods for reprocessing silicon carbide. While SiC was reported to be volatilized in chlorine gas under $SiCl_4$ form or through reaction with water vapor to form volatile species such as $Si(OH)_4$. [6, 9] However, the volatilization rates of SiC in both processes are too low to be applied in industry. Electrochemical and plasma etching require specialized equipment which is incompatible with equipment and processes used in the nuclear industry. Besides, the etching rate is low in the micrometer scale per hour. [10-12]

Molten salt corrosion is a process in which molten salts corrode the surface they contact with. [6, 13-14] This method was selected since it allows for dissolution of SiC inert matrix fuel at a considerable rate without limitations of pellet size and processing batch size. This work focuses on using a molten salt involved reaction/dissolution to separate a surrogate for Pu from SiC inert matrix and investigating the factors which affect the reaction rate in order to optimize the design of separation condition.

The selection of molten salts was conducted based upon a literature survey. Powder and bulk SiC samples which are commercially available were tested to verify the feasibility of the separation method. The same experiment was conducted on ceria, a surrogate for plutonium and minor actinides, to confirm that no weight or phase change of ceria under the tested corrosion condition. Plutonium and minor actinides, due to their radiotoxic nature, are difficult to handle in lab.

SiC pellets with and without ceria were fabricated in this lab at a temperature which is lower than the temperature for fabrication of the mixed oxide fuels in the nuclear industry. The microstructure analysis on the SiC samples before and after corrosion was performed using scanning electron microscopy (SEM). The phase and composition of SiC samples and the corrosion product was identified by X-ray diffraction (XRD), Inductive Coupled Plasma (ICP) and Energy Dispersive Spectrometry (EDS).

Multiple parameters were investigated in order to understand the mechanism of the molten salt reaction with bulk SiC and to determine the optimal condition for reprocessing SiC IMFs. After the desirable reprocessing condition was selected, the SiC pellets with ceria were tested to determine if the separation of ceria from SiC inert matrix is achieved.

1.3 Organization of Dissertation

In Chapter 2, a brief background is provided for topics pertinent to the research presented in the following chapters. The contents covered in this chapter include an introduction to the inert matrix fuels (IMF) and proposed reprocessing methods for the current inert matrix candidates. The properties of SiC as an inert matrix and the methods of SiC fabrication are introduced. The possible routes for reprocessing SiC IMFs are reviewed.

In Chapter 3, the reprocessing method, type of SiC specimens and salts were selected. The procedures for fabrication of SiC pellets at a low temperature are described. The process for reprocessing SiC IMFs was developed. Characterization techniques are used to examine the particle size distribution of starting powder, the crystal structure and the composition of samples and products and microstructure of the SiC specimens before and after corrosion.

In Chapter 4, SiC powder is tested to assess the feasibility of reprocessing SiC by using the molten salt reaction/dissolution method. The effects of molten salt depth and salt amount on the reaction rate of SiC pellets are investigated. The SiC reaction kinetics in two different salts is studied. The controlling factor for SiC corrosion in molten salts at 1050 ºC is proposed. In Chapter 5, multiple oxidizing gases and different combination of gases were evaluated in order to optimize the process.

In Chapter 6, the weight and phase changes of ceria powder and pellets in two salts under various atmospheres are examined. Ceria is separated from the SiC/ceria composites in the proposed reprocessing conditions. The amount of ceria recovered from this process and its crystal structure are examined. In Chapter 7, the presented dissertation is summarized and a proposal for future work is discussed.

CHAPTER 2
BACKGROUND

A brief review of concepts and background is provided in this chapter to understand the research discussed in the following chapters. The important properties of SiC as an IM candidate are included in this chapter as well. The available SiC degradation methods are summarized at the end.

2.1 Inert Matrix Materials and Their Reprocessing Techniques

Destruction of plutonium and minor actinides is the basic aim for the IMF applications. Following are properties which a potential IMF material should possess [1, 5, 15]:

1. Neutron properties, for example, low neutron adsorption cross section to achieve high burn-up of fuels. Neutron transparency is the basic requirement for the inert matrix materials in order to overcome the problem of UO_2 based MOX fuels.
2. Good compatibility with the coolant and structural materials. The IM materials should be chemically inert when contacting with cladding materials such as Zircaloy and stainless steel and coolant such as water and sodium in order to maintain their properties during performance.
3. Good thermo-physical properties such as thermal conductivity and heat capacity to minimize the centerline temperature and to maximize the safety margin.
4. Optimal properties after irradiation against neutrons, alpha decay and fission fragments; for example, phase stability, minimum swelling and constant mechanical strength.

A list of the IMF candidates is summarized in Table 2-1, based on the available material screening in the current literature. [1] After burning in the light water reactors in which light water is used as the coolant and neutron moderator, the used IMFs can be reprocessed for a later irradiation or directly sent for geological disposal. Geological storage without reprocessing requires that the inert matrix material should be chemically stable for a long time e.g. thousands of years. [5] The used IMFs are not suitable for

long term storage due to concern of proliferation risks and environmental safety. Moreover, substantial energy can be extracted from the used fuels after reprocessing during a transmutation process. [3] Although reprocessing of the spent fuels in the commercial nuclear program has been forbidden in USA since the mid-1970s due to a proliferation concern, reprocessing spent fuels has been proposed in the Global Nuclear Energy Partnership (GNEP) and the Advanced Fuel Cycle initiative (AFCI).[3]

Before introducing the strategies for reprocessing IMFs, two current routes to reprocess spent nuclear fuels are reviewed. Both approaches require the spent nuclear fuels to dissolve in nitric acid before separation. The first method is called plutonium and uranium recovery by extraction which is abbreviated as PUREX. In this process, plutonium and U are extracted from the solution through complexing by tributyl phosphate (TBP). Fission fragment and minor actinides are left in the solution. The other method is called uranium recovery by extraction (UREX). Pu and Np are complexed by using acetohydroxamic acid (AHA) in order to prevent them being extracted. Uranium and Tc are separated from the solution but the transuranium (TRU) isotopes and fission products are rejected to the aqueous raffinate. The aqueous treatment has been a mature technique for reprocessing the used fuels. It is desired to transfer this method to IMFs.

Techniques of reprocessing the IMF candidates have been studied for several decades. For example, pyrochemical reprocessing is suitable for degrading the metallic inert matrices such as ZrC and TiC. [6] In this process, the inert matrix materials are fed into a bath of molten chloride salts and volatized under tetrachloride forms leaving the transuranic fuels intact. However, solid carbon remaining in the salts is difficult to

eliminate. In another separation method developed recently, high purity chlorine gas is used to chlorinate the metallic carbides at 400 ºC [6, 16]. The remaining solid carbon is removed by oxidation under O_2 at 400 ºC. Since reprocessing the spent nuclear fuels in an aqueous solution is a mature technique in which Pu and minor actinides can be separated from U and other fission fragments, some researcher suggest using an aqueous method to reprocess the spent fuels and the used IMFs. [17] Binary metal oxide such as MgO and Y_2O_3 were reported to completely dissolve in nitric acid (HNO_3) which is widely used in the current reprocessing techniques. [3, 18]

2.2 Evaluation of SiC as an Inert Matrix

2.2.1 Radiation Tolerance

Silicon carbide with high purity and good stoichiometry after irradiation has been extensively studied in order to identify the irradiation-induced changes of mechanical properties [7, 19-24], dimension [21, 24-26] and thermal conductivity [7, 19, 21, 23, 27-28]. Increasing the irradiation dosage and decreasing the irradiation temperature in a range of 400 ºC to 800 ºC can cause fracture toughness of SiC increases. [24] One possible mechanism of irradiation toughening is that fracture energy dissipates at the sites of micro-cracks induced by irradiation. [19-20, 24] However, the physical properties such as elastic modulus, hardness of the irradiation damaged site decreased because of the amorphization and disordering of SiC by neutron irradiation. [22, 29]

Thermal conductivity of SiC is significantly reduced due to surface amorphization after fast-neutron irradiation. [21, 26, 30] Moreover, the lattice vacancies which serve as the phonon scattering centers can be generated during neutron irradiation, reducing SiC thermal conductivity as a result. For example, the un-irradiated CVD SiC at room temperature has a high thermal conductivity at 256 $Wm^{-1}K^{-1}$. Irradiation to 0.1dpa

reduces thermal conductivity to 31 $Wm^{-1}K^{-1}$, which, however, is still higher than UO_2 which has thermal conductivity lower than 10 $Wm^{-1}K^{-1}$. [7, 21, 25] Silicon carbide shows good swelling resistance. The maximum swelling of SiC irradiated by the fast neutrons at room temperature has been reported at 1.24%. [22, 26, 31] The amount of swelling monotonically decreases with increasing the irradiation temperature. [26]

2.2.2 Hydration Resistance

To apply in the LWRs, the IM materials should exhibit high resistance to the circulating water coolant at 300 ºC, which is the operating temperature of many water-cooled reactors. [32] Charles found pitting corrosion of CVD SiC after exposing in the de-oxygenated water up to 5400 h at 300 ºC and 10 MPa. [32] Silicon loss in the pitting area may be attributed to dissolution of the silica protective layer and formation of water-soluble silicon hydroxide:

$$SiO_2 + H_2O \rightarrow H_2SiO_3^- + H^+ \rightarrow SiO_3^{2-} + 2H^+ \quad (2\text{-}1)$$

$$SiC + 4H_2O \rightarrow Si(OH)_4 + CH_4 \quad (2\text{-}2)$$

$$Si(OH)_4 \rightarrow H_3SiO_4^- + H^+ \rightarrow H_2SiO_4^{2-} + 2H^+ \quad (2\text{-}3)$$

The rate of pitting corrosion depends on the oxygen activity and pH of the water. No weight loss of SiC was observed after exposure for 5400 h in the reported experiment condition. [32] This corrosion process is much slower compared to other IM candidates such as MgO based materials. [33]

2.2.3 Thermal Conductivity

Thermal conductivity of SiC varies significantly in a range from 31 to 490 $Wm^{-1}K^{-1}$ depending on the fabrication routes. [7] The approximate value of the centerline temperature of SiC IMF can be estimated by using the following formula:

$$P = 4\pi \int_{Ts}^{Tc} \kappa dT \quad (2\text{-}4)$$

where P is the linear power of the fuel elements and Tc and Ts are the centerline and the surface temperature of the fuel. Given the linear element power 55 kWm^{-1} which is the peak power of a CANDU reactor and the surface temperature at 300 ºC, the centerline temperature of the neutron-irradiated SiC IMF can be calculated as 827 ºC. [7] This temperature is still considerably lower than the central temperature of the UO_2 fuel (1500 ºC) under the same irradiation condition. [7]

2.3 SiC Fabrication Techniques

In order to understand which method of SiC sintering is more compatible with the current fabrication techniques of the nuclear fuel pellets utilized in the nuclear industry, it is necessary to review the conventional processes of fabrication of the UO_2 and MOX fuel and the SiC sintering techniques. In a fuel fabrication plant, uranium hexafluoride (UF_6) is enriched by separating the uranium isotope U^{238} from U^{235} which most readily fissions in the light water nuclear reactors. UF_6 is converted to uranium dioxide (UO_2) ceramic powder after enrichment, followed by uniaxially pressing the powder into pellets and sintering in a furnace at a high temperature usually around 1600 ºC. To fabricate the MOX fuels, UO_2 and PuO_2 powder are first blended to form a homogenous mixture (95% UO_2 and 5% PuO_2) in which PuO_2 is uniformly dispersed. The mixture is compressed into a pellet shape and sintered in a furnace at 1700 ºC.

Commercialized SiC can be categorized into several types according to the fabrication processes: direct-sintered (DS), hot-pressed (HP), chemical vapor deposited (CVD) and reaction-bonded (RB) SiC. Direct sintering begins with preparation of a slurry consisting of sub-micron SiC powder, sintering aids, carbon sources and binders.

Sintering is carried out in an atmosphere-controlled vacuum furnace at temperature above 2000 ºC. Hot pressing a homogenous dispersion of SiC submicron powder and the sintering additives is accomplished above 2000 ºC under pressure in a range of 30 to 70 MPa. Full densification and a uniform microstructure of SiC can be obtained in this process. In the CVD process, a mixture of methyltrichlorosilane (CH_3SiCl_3) vapor and hydrogen is transported into a reaction chamber which contains a heated graphite rod. When contacting with the hot rod, the silane decomposes and silicon carbide is deposited. Reaction bonded SiC is also commonly called high free silicon-silicon carbide. Usually, fabrication starts with preparation a mixture of SiC particles and graphite powder. After pressing or extruding into the desired shapes, the samples in contact with molten silicon (melting point: 1414 ºC) are placed in an atmosphere-controlled furnace. Secondary SiC is formed as a bond phase because of the reaction between graphite and the silicon melt.

Another SiC sintering method is called liquid phase sintering (LPS). [7, 34] This process includes preparation of a homogenous mixture of SiC powder and the sintering additives such as Al_2O_3 and Y_2O_3, uniaxial pressing powder into the green compacts and pressure-less sintering in an inert atmosphere at temperature lower than 2000 ºC. During this sintering process, yttrium-aluminum-garnet (YAG) is generated as an intergranular phase among the SiC particles. YAG melting is believed to enhance diffusion and transportation of the SiC particles and other species, resulting in SiC full densification at a comparatively lower temperature.

Polymer impregnation and pyrolysis (PIP) is an alternative route to produce less dense SiC which has a relative density in a range of 80% - 90%. [35-37] SiC bulk

density depends on the number of cycles of polymer infiltration. The PIP process consists of the following steps:

1. A mixture of a polymer precursor and SiC powder usually in micron size is pressed into the green compacts and sintered under an inert atmosphere such as argon (Ar) or nitrogen (N_2).
2. During heat treatment, the polymer precursor decomposes to form amorphous or crystalline β-phase SiC depending on the firing temperature. Initial SiC particles in the green compacts are connected by a polymer-derived SiC network.
3. More polymer precursors can be impregnated into the open pores of the fired SiC pellets for another pyrolysis cycle in order to increase SiC density.

A commonly used polymer precursor to yield near stoichiometric SiC is allyl-hydrido-poly-carbo-silane which is a commercially available product named SMP-10 and has the elements Si and C at a 1:1 molar ratio on the resulting ceramic. The recommended firing steps and product information are provided by the vendor Starfire Inc. The precursor becomes cross-linked at the curing stage in the temperature range of 180 ºC to 500 ºC. Amorphous SiC is formed at 850 ºC -1200 ºC and nano-crystalline β-SiC forms at higher temperature ranging from 1250 ºC to 1650 ºC.

Four commercialized processes (DS, HP and CVD) for SiC fabrication require either very high temperature facilities or specialized equipment and process. The existing fuel fabrication lines can be easily adapted to the reaction bonded process, liquid phase sintering and polymer precursor sintering. However, a large amount of Si metal phase can be generated in the reaction bonded process. The amount of sintering additives needed in the LPS is also considerable (7-30 wt%). [7, 34] Both will affect performance of the SiC inert matrix in the LWRs. The fissile atoms may diffuse in either the liquid Si phase or the liquid garnet phase at high irradiation temperature, which makes microstructure of the sintered IMF pellets difficult to control. Therefore, the PIP

method was chosen in this work to fabricate the SiC samples for the study of reprocessing SiC IMFs.

2.4 Possible Strategies for Reprocessing Silicon Carbide

2.4.1 Oxidation

Silicon carbide is a thermodynamically unstable ceramic when exposed to an oxidizing atmosphere. SiC is considered to be practically stable due to the slow rate of oxidation at low temperature. The oxidation behaviors of SiC in different oxidizing gases are discussed as below.

2.4.1.1 Oxidation in dry oxygen

In presence of oxygen with moderate and high partial pressure, a thin silica layer is formed [38-42]:

$$SiC(s) + \frac{3}{2}O_2(g) \rightarrow SiO_2(s) + CO(g) \quad (2\text{-}5)$$

As the silica film develops, it retards the oxidation process because of the low oxygen diffusivity in silica. This reaction which is known as passive oxidation usually follows parabolic kinetics. If oxygen at a low partial pressure SiC is oxidized into gaseous species, which is known as active oxidation:

$$SiC(s) + O_2(g) \rightarrow SiO(g) + CO(g) \quad (2\text{-}6)$$

Y. Song reported a pressure (O_2)-temperature phase diagram for SiC oxidation in O_2, which consists of three distinct regions: graphitization, active oxidation and passive oxidation. [43] Graphitization occurs at very high temperature and sufficiently low O_2 pressure:

$$SiC(s) + O_2(g) \rightarrow Si(g) + CO(g) + C(s) \quad (2\text{-}7)$$

With increasing the concentration of O_2, carbon is no longer present:

$$SiC(s) + O_2(g) \rightarrow Si(g) + CO(g) \quad (2\text{-}8)$$

Active oxidation dominates at higher O_2 pressure. Passive oxidation occurs when O_2 pressure is considerably high. In conclusion, the condition of active oxidation should be achieved in order to continuously degrade SiC.

2.4.1.2 Oxidation in water vapor

SiC can be oxidized by H_2O in a combustion environment [44-47]:

$$SiC(s) + 3H_2O(g) \rightarrow SiO_2(s) + CO(g) + 3H_2(g) \quad (2\text{-}9)$$

The SiO_2 layer can be removed through reactions to produce volatile silicon monoxide, hydroxide or oxyhydroxides:

$$SiO_2\ (s) + H_2(g) \rightarrow SiO(g) + H_2O(g) \quad (2\text{-}10)$$

$$SiO_2\ (s) + CO(g) \rightarrow SiO(g) + CO_2(g) \quad (2\text{-}11)$$

$$SiO_2\ (s) + H_2O(g) \rightarrow SiO(OH)_2(g) \quad (2\text{-}12)$$

$$SiO_2\ (s) + 2H_2O(g) \rightarrow SiO(OH)_4(g) \quad (2\text{-}13)$$

$$SiO_2\ (s) + 3H_2O(g) \rightarrow Si_2O(OH)_6(g) \quad (2\text{-}14)$$

$$SiO_2\ (s) + \frac{1}{2}H_2O(g) \rightarrow SiO(OH)(g) + \frac{1}{4}O_2(g) \quad (2\text{-}15)$$

$$SiO_2\ (s) + 3H_2O(g) \rightarrow Si_2(OH)_6(g) + \frac{1}{2}O_2(g) \quad (2\text{-}16)$$

Water vapor significantly enhances the oxidation of SiC even without other oxidizers such as oxygen. [48-49] The rate of SiC volatility was found to be proportional to the root of water vapor velocity. [50] SiC exposure to wet and dry air at 1200 ºC resulted in different silica layer thicknesses. [50] Only a thin, dense silica layer formed in dry air. Scale-thickness measurement is not necessarily reliable in determining the amount of SiC oxidation because of scale spallation and incorporated defects such as cracks and voids. Specific weight change measurements shown in Figure 2-1 [48] are

often used to calculate the SiC oxidation rate coefficient and to establish the kinetic models. The parabolic rate constant (k_p) is usually approximated by the classical parabolic equation [51]:

$W^2=k_{pt} + b \approx k_{pt}$

$W = \Delta W/A$: the weight change per unit area (mg cm^{-2}) at a certain time t;

k_p: the parabolic rate constant $k_p=k_{p0}exp(-Ea/RT)$ ($mg^2cm^{-4}h$);

b: a constant attributed to the effect of a possible non-parabolic initial stage, for instance, which does not have an exact definition when t equals zero.

Water significantly enhances k_p because it depends on oxidizer diffusivity (D) and solubility (C) in the SiO_2 layer. [44-47] It was reported that while $D(H_2O)$ is a little less than that of O_2, $C(H_2O)$ is 50 times higher than O_2. [48] A linear relationship between time and weight change per area in Figure 2-1 [48] is indicative of the parabolic oxidation kinetics. Various water vapor pressures accelerate SiC oxidation at different rates from 1100 ºC to 1400 ºC compared to the dry oxygen atmosphere shown in Figure 2-2 [48]. The elevation of water-vapor partial pressure results in the silica growth rate increasing.

The mechanism of oxidation enhancement due to water addition is still ambiguous. Two hypotheses have been provided: [52]

1. At high temperature, water molecules may decompose into hydroxyl which have sufficient activity to oxidize SiC;
2. Water molecules may act as a carrier gas for oxygen because water has a high solubility in SiO_2. Once reaching to the SiC surface, oxygen is released from water to react.

Observations in the available experiment tend to support the first hypothesis, since the results of SiC and Si oxidation in H_2O/argon mixtures are not statistically differentiated

from those obtained in the H_2O/O_2 mixture. [48-49] The temperature at 1050 ºC has been reported as the lowest temperature at which water vapor has an obvious enhancement on SiC oxidation compared to pure oxygen.[53-54]

2.4.1.3 Oxidation in dry carbon dioxide

The passivating layer can also be generated in an atmosphere containing carbon dioxide [55-56]:

$$SiC(s) + 3CO_2(g) \rightarrow SiO_2(s) + 4CO(g) \quad (2\text{-}17)$$

SiC weight increasing in CO_2 at 1473 K has been reported to follow the parabolic-like kinetics. [55] The oxidation rate is approximately 20 times slower in CO_2 than in O_2, dependent on temperature and independent of the CO_2 partial pressure. [55] The low oxidation rate is understandable since the CO_2 molecule (3.94 Å) is larger than the O_2 molecule (3.47 Å) if SiC oxidation in CO_2 is limited by gas diffusion. When the temperature was increased up to 1500 ºC, SiC weight loss began after a certain amount of weight gain. [55] This phenomenon may be due to interaction at the SiC/SiO_2 layer and formation of the volatile SiO:

$$2SiO_2 + SiC = 3SiO(g) + CO(g) \quad (2\text{-}18)$$

The kinetics of SiC weight change in CO_2 is shown in Figure 2-3 up to 100 h at various temperatures [55]. At 1200 ºC, the average parabolic constant estimated at 3×10^{-6} $mg^2/(h \cdot cm^4)$ is much less significant than the constants of O_2 and 50% H_2O/O_2 which are on the order of 1×10^{-4} $mg^2/(h \cdot cm^4)$ and 1×10^{-3} $mg^2/(h \cdot cm^4)$, respectively. The SiC weight change rates in three types of atmospheres were compared in Figure 2-4. [55]

2.4.1.4 Oxidation in ozone

Ozone gas (O_3) with a higher oxidizing activity than O_2 has been used to oxidize SiC. [57-58] Rapid oxidation may be attributed to dissociation of the ozone gas:

$$O_3(g) = O_2(g) + O \quad (2\text{-}19)$$

The oxidation rate may be limited by diffusion of atomic oxygen through the SiO_2 layer, since the parabolic constant has been found to increase linearly as the ozone partial pressure increased at 600 ºC. [57] The oxidation rate is higher at the SiC carbon face than at the SiC silicon face. This result is believed to because the formation of CO gas which is rapidly removed from the SiC/O_3 interface. When the temperature increases to 827 ºC, no oxidation enhancement in ozone is observed compared to oxidation in dry oxygen. [57] This may be because the O_3 transforms into O_2 molecules:

$$O_3(g) = \frac{3}{2}O_2(g) \quad (2\text{-}20)$$

Ozone gas as an oxidizer of SiC is more efficient than oxygen at low temperature.

2.4.2 Chlorination

SiC can be attacked by chlorine gas (Cl_2) at high temperature (e.g. above 900 ºC) to form a volatile product $SiCl_4$ and solid carbon [6, 16]:

$$SiC(s) + 2Cl_2(g) = SiCl_4(g) + C(s) \quad (2\text{-}21)$$

Bourg found that SiC powder in micron size has a significant weight loss under Cl_2 gas at 900 ºC, as shown in Figure 2-5. [6] The weight of the SiC sample changes linearly as a function of the chlorination time. If all the Si can be volatized under the $SiCl_4$ form and carbon remains, the maximum theoretical weight loss of the SiC sample is 70%. [6] Carbon can be removed by oxidation in oxygen at 400 ºC.

2.4.3 Molten Salt Corrosion

Molten salt corrosion is a process in which the molten salts corrode the surfaces which they come into contact. In research on the gas turbine engine degradation and the coal combustion process, SiC corrosion was observed in the presence of the carbonate and sulfate salts of sodium (Na) and potassium (K), because the ceramic surface is quickly attacked by the condensation of the Na, and K impurities that are present in the gaseous environment. [13, 59-64]

SiC is usually covered by a thin silica layer which protects it from further oxidation. When exposed to the molten salts, silica is easily attacked to form the crystalline or molten silicates. Since the silicates have lower density compared to silica, both diffusivity and solubility of the gaseous oxidizers in the silicates is large enough to allow further oxidation and corrosion of SiC. It has been predicted that once the silicate layer grows to a critical thickness and the temperature is sufficiently low, the molten salt ions may not pass through the thick silicate layer, resulting in termination of corrosion. [61, 63] If the temperature is considerably high, for example, above the melting temperatures of silicates, the alkali silicate layer will be dissolved in the molten salt. [65]

2.4.3.1 Molten carbonates

Sodium carbonate (Na_2CO_3) is known to react with silica (SiO_2) forming sodium silicates: [59, 66]

$$Na_2CO_3(l) + SiO_2(s) = Na_2SiO_3(s) + CO_2(g) \quad (2\text{-}22)$$

ΔG_0 = -79.9 kJ/mol at 1000 ºC

Aled R. Jones et al. identified and quantified the Na_2CO_3 and SiO_2 (quartz) reaction products and intermediates in a temperature range from 700 ºC to 1300 ºC. [65] Those

products were quenched in air to decrease devitrification of the melt phase. At 950 ºC, crystalline sodium silicate (Na_2SiO_3) with a melting temperature of 1090 ºC is predominant in the melt [65], which indicates that Na_2SiO_3 is the most stable product at this temperature. Additionally, the mixture of crystalline Na_2SiO_3 and glassy silicate were observed after an isothermal reaction for 45 minutes at 1090 ºC as a result of crystalline Na_2SiO_3 melting. Furthermore, a decelerating reaction to form Na_2SiO_3 was reported [13, 61, 65], indicating that the reaction is diffusion limited. Since the crystalline silicate is formed at the interface between SiO_2 and the molten salt, the continuation of the reaction requires the mobile sodium ions to transport across the increasing layer of crystalline sodium silicate. The amount of Na+ diffusing through the interface decreases as the silicate layer increases.

2.4.3.2 Molten sulfates

The corrosion mechanism of SiC in sodium sulfate is similar to the sodium carbonate case. However, the reaction between silica and sodium sulfate is unfavorable at 1000 ºC or higher, especially at a high SO_3 partial pressure (greater than 0.1 Pa): [61, 63-64, 67]

$$SiO_2(s) + Na_2SO_4(l) = Na_2SiO_3(s) + SO_3(g) \quad (2\text{-}23)$$

ΔG_0 = 147.5kJ/mol at 1000 ºC

If a flowing gas other than SO_3 such as Ar or O_2 removes SO_3 immediately once it is produced, sodium silicate can still be generated. [61]

Moreover, it has been observed that SiC would experience severe corrosion in SO_3/O_2 atmosphere if SiC contains extra carbon. [61] The carbon enhanced corrosion is formulated as follow:

$$SiO_2(s) + Na_2SO_4(l) + 2C(s) + \frac{3}{2}O_2(g) = Na_2SiO_3(s) + SO_2(g) + 2CO_2(g) \quad (2\text{-}24)$$

$$SiO_2(s) + Na_2SO_4(l) + 4C(s) + \frac{3}{2}O_2(g) = Na_2SiO_3(s) + SO_2(g) + 4CO(g) \quad (2\text{-}25)$$

The silicate layer grows as time increases until the critical thickness is reached where the layer is too thick to be penetrated. [61, 64]

2.4.3.3 Molten chloride

SiC is resistant to the molten chloride salts such as potassium chloride (KCl) under an inert atmosphere. [68] In presence of the oxidant gases O_2, or H_2O, SiC is corroded in the chloride salt to form the water soluble silicates: [68]

$$2KCl(g) + SiC(s) + \frac{3}{2}O_2(g) = K_2SiO_3(l) + CO_2(g) + Cl_2(g) \quad (2\text{-}26)$$

$$2KCl(g) + SiC(s) + 2O_2(g) + H_2O = K_2SiO_3(l) + CO_2(g) + 2HCl(g) \quad (2\text{-}27)$$

Weight loss of SiC samples increases linearly as the reaction time increases. Increasing temperature can accelerate the corrosion process. However, the SiC corrosion rate in the molten chlorides is considerably less than that in the molten sulfate and carbonate salts. [6, 68]

2.4.4 Etching

Wet etching and plasma etching are the common methods to etch SiC. Wet etching can be divided into two categories: chemical and electrochemical etching. Both methods require an aqueous solution except that an external voltage source is needed for the latter. Since SiC has excellent chemical inertness due to the protective oxide layer, the efficient etching has been achieved so far in $K_3Fe(CN)_6$ solution above 100 ºC and in phosphoric acid at 215 ºC. [11, 69] However, a layer of silica is left on the SiC surface after etching in phosphoric acid, causing the reaction to terminate. Carbon phase is not attacked in $K_3Fe(CN)_6$ solution. Solutions which have been used in

electrochemical etching SiC are hydrofluoric acid (HF), sulfuric acide (H_2SO_4), hydrochloric acid (HCl), sodium hydroxide (NaOH), potassium hydroxide (KOH) and hydrogen peroxide (H_2O_2). [10-11] While the solution choice is multiple, the etching facility is not compatible with the equipment in nuclear industry.

Plasma etching also can be divided into two categories: reactive ion etching (RIE) and inductively couple plasma etching (ICPE). [12] Plasma etching is also known as dry etching, where SiC is exposed to bombardment of the accelerated ionized gas molecules such as fluorocarbons, mixed with oxygen or argon and etched directionally or anisotropically. Both etching methods allow SiC to be etched at much lower temperature compared to the aforementioned molten salt corrosion and oxidation but, the etching rates are less than 1 μm/min. [10-12]

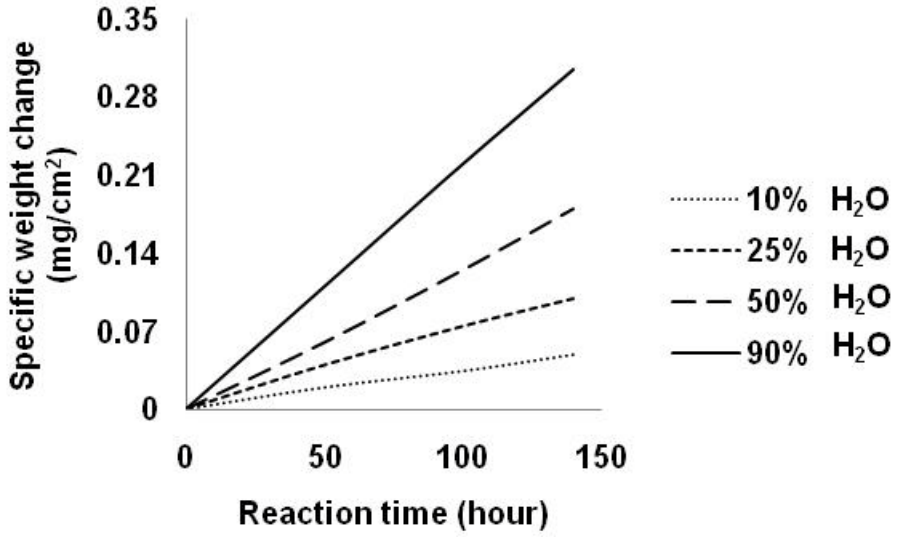

Figure 2-1. Determination of the parabolic rate constants for CVD SiC in H_2O/O_2 mixtures at a total pressure of 1 atm and a temperature of 1200 ºC [48]

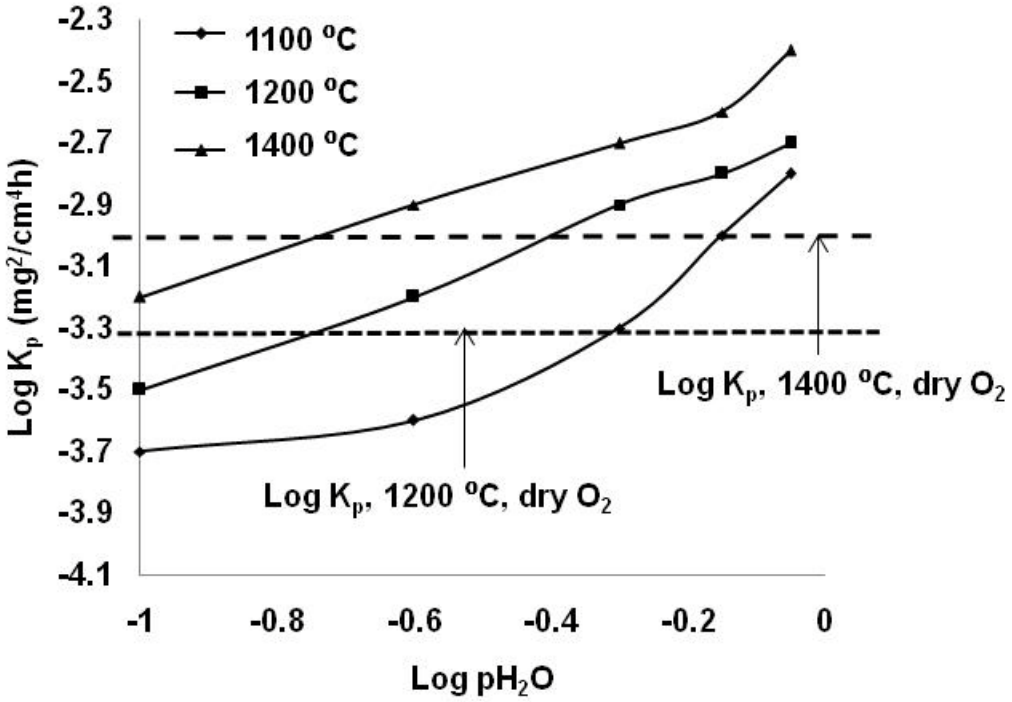

Figure 2-2. Water-vapor-pressure dependence of the parabolic oxidation rate constant for CVD SiC in 1100 ºC -1400 ºC in H_2O/O_2 mixtures at 1atm [48]

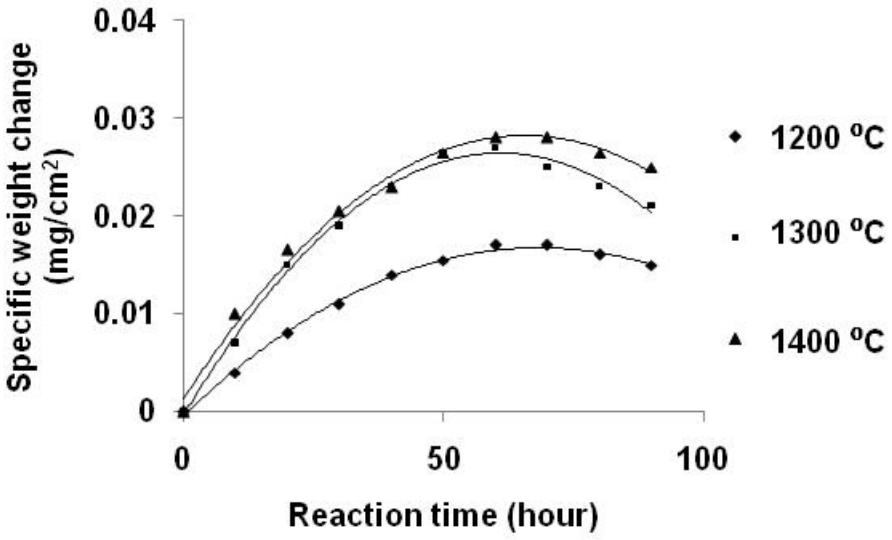

Figure 2-3. Oxidation weight change kinetics of CVD SiC at different temperatures as a function of time [55]

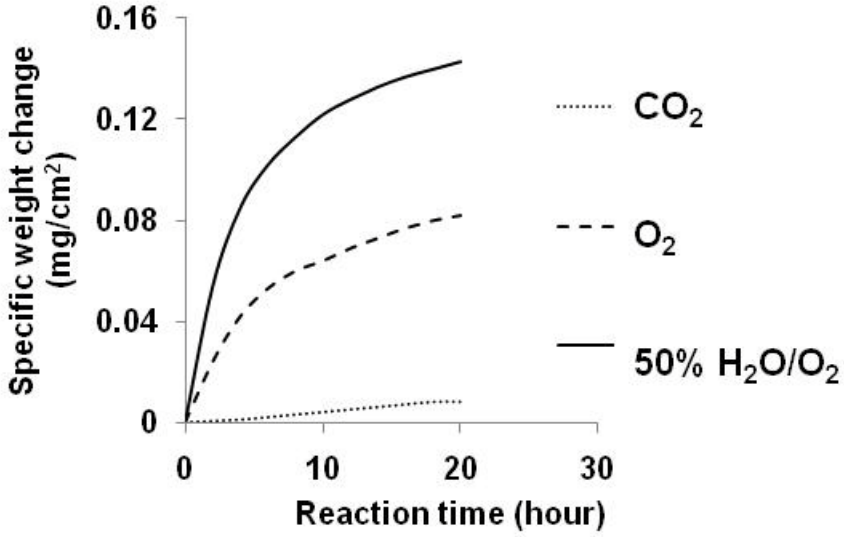

Figure 2-4. Oxidation weight change kinetics of CVD SiC in different atmospheres as a function of time at 1200 ºC [55]

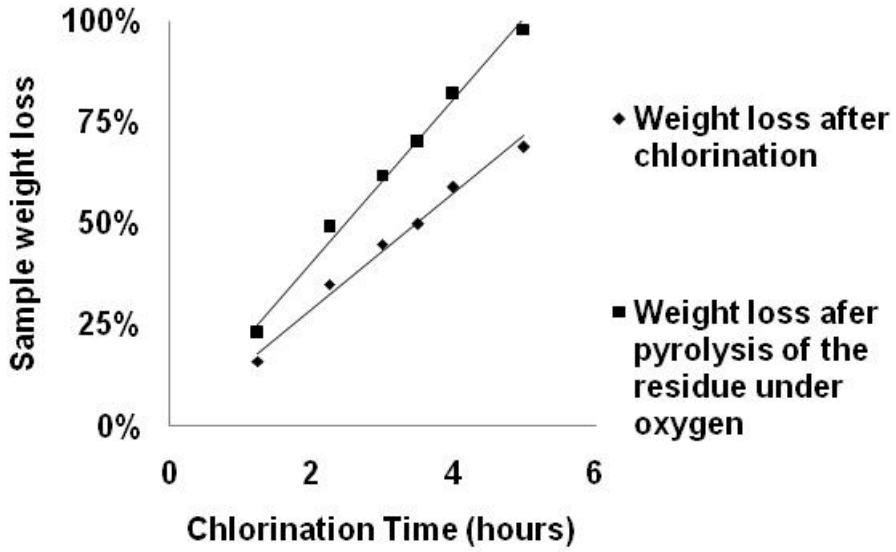

Figure 2-5. Weight loss of SiC powder (400 mg, 45 μm) as a function of the chlorination time at 900 ºC [6]

Table 2-1. Examples of inert matrix, additive candidates and their design [1]

Inert matrix components	Inert matrix formula
Carbides	SiC, TiC, ZrC
Binary oxides	MgO, CaO, Y_2O_3, ZrO_2
Oxide solid solutions	$Ca_xZr_{1-x}O_{2-x}$, $Y_yZr_{1-y}O_{2-y/2}$

CHAPTER 3
SELECTION OF REPROCESSING ROUTE AND MATERIALS, PROCESS DESIGN, EXPERIMENTAL PROCEDURES AND CHARACTERIZATION

3.1 Introduction

This chapter begins by discussing the selection criteria for the SiC samples, reprocessing methods and molten salts used in this research. The gas supplying facility design, the procedures for synthesizing and reprocessing the SiC specimens are described. The characterization tests on the initial SiC specimens and the products are introduced.

3.2 Selection of SiC Types, Reprocessing Method and Molten Salts

3.2.1 Selection of SiC

The common polymorphism of silicon carbide can be categorized into two types: α-SiC and β-SiC. α-SiC has a hexagonal crystal structure which is formed above 1700 °C. β-SiC has a zinc blende crystal structure which is formed below 1700 °C. β-SiC has a larger thermal conductivity which is approximately 420 W/m•K than the α-SiC which is in a range of 260 to 300 W/m•K. [30] β-SiC has an isotropic structure. The thermal conductivities along both directions are identical. α-SiC has a long-period hexagonal structure in which thermal conductivity parallel to the c-axis was reported as 30% less than that perpendicular to the c-axis. [70] Although all polytypes of SiC have very low coefficients of thermal expansion, the isotropic crystal structure is generally desired in the nuclear industry application in order to prevent crack formation in the SiC matrix and the SiC/cladding interface due to anisotropic swelling. [26]

3.2.2 Selection of Reprocessing Method

Several possible SiC reprocessing methods were reviewed in chapter 2. Molten salt corrosion was chosen in this work because of the following reasons:

1. Equipment used in the molten salt reaction/dissolution strategy is compatible with the current facility of manufacturing nuclear fuels.

2. Reaction rate is comparatively high.

3. Salt choices are multiple, e.g. sodium carbonate (Na_2CO_3), potassium carbonate (K_2CO_3), sodium nitrate ($NaNO_3$), sodium sulfate (Na_2SO_4) and potassium chloride (KCl).

3.2.3 Selection of Molten Salts

Alkali (Li, Na and K) carbonates, nitrates, chlorides and sulfates have been widely reported to severely corrode silicon carbide, since they have basic anions such as O^{2-}, CO_3^{2-}, Cl^-, SO_4^{2-} and NO_3^- which can react with the silica layer forming alkali silicates. [6, 61, 63, 67] The following criteria were applied in this work to select the desired molten salts:

1. Producing water soluble silicates. The reprocessing strategy in this work is dissolving the SiC matrix in a liquid but leaving the fuels as intact solids.

2. No reaction with PuO_2. Reprocessing the SiC IMFs is to recycle the non-transmutated fuels. New phase generation in the fuels will cause complexity in recycling.

3. Low melting point e.g., below 1200 °C. Reactive ions and molecules diffuse faster in the salt melts than in their solid phase. Choosing a salt with low melting point will reduce the processing temperature. Moreover, the commercialized high temperature furnaces are usually classified into 1100 °C-1200 °C, 1500° -1600 °C, 1700 °C-1800 °C and higher, depending on the maximum operating temperature. The expense of those furnaces increases dramatically as increasing the maximum operation temperature range. Therefore, the maximum processing temperature is set at 1200 °C in this work based on the economical consideration.

4. High boiling point e.g., above 1200 °C. Salt boiling during the reaction process is undesired since it causes considerable salt loss and environmental contamination.

5. Generating no or less corrosive gas products due to salt decomposition or salt/SiC reaction. The corrosive gases such as NO_2, SO_2, and SO_3 will cause equipment damage and safety issues especially in the presence of moisture.

6. Rapid reaction with SiC. The corrosion rate should be sufficiently high to be applicable in the nuclear industry.

Since only sodium silicates and potassium silicates have significant solubility in water, the choices are limited to the Na and K salts. Several sodium and potassium salts, their relevant properties and corresponding evaluations are summarized in Table 3-1. The boiling temperature of hypochlorites, chlorates and nitrates are too low to be considered. The reaction rates in the fluoride and chloride salts were reported to be significantly low due to the less basic nature of the non-oxygen ions. [6, 71] No phosphate salts/SiC reaction has been reported. Hydroxides are not desirable due to the caustic nature. Bicarbonates decompose dramatically at very low temperature forming carbonates, water and carbon dioxide. The acid gases such as SO_2 and SO_3, generated during corrosion in the sulfate salts are highly corrosive to equipment. Therefore, sodium carbonate and potassium carbonate were selected in this work to reprocess the silicon carbide IMFs.

3.3 Process Design

A scheme of process design was illustrated in Figure 3-1. Air, argon, carbon dioxide, and oxygen were supplied through the compressed gas cylinders. A twin flow meter was used to adjust gas flow. The pressure change in the system was monitored by using a vacuum/pressure gauge. A tube furnace (Model F79340-33 manufactured by Barnstead Thermolyne) with stain-less steel caps on both ends was used in the SiC corrosion studies. The tests were conducted at 900 ºC and 1050 ºC. A uniform temperature zone was approximately 4 inch long measured by using a k-type thermocouple at the midway along the tube furnace. Nano-pure water contained in syringes was supplied through a syringe pump. At 1050 ºC, the end-cap temperature was above 200 ºC which allowed water to vaporize immediately once it was pumped into the furnace. A glass wool plug was placed near the inlet end to equilibrate the water

vapor flow. The partial pressure of water vapor in the gas mixture was varied by controlling the liquid water flow rate. To assure an accurate quantification of the corrosion rate under different gas atmospheres at 1050 ºC, little reactive gas such as O_2, H_2O and CO_2 exists in the tube furnace at the heating ramp stage. Moreover, corrosion needs to be rapidly terminated after a certain isothermal holding period. Both conditions were achieved by pumping out the reactive gases by using a vacuum pump, followed by applying UHP Ar gas in the tube furnace. Outflow gases were bubbling through two different liquids in order to monitor if any block was formed in the tubing due to salt condensation. Silicon oil was used in non-water vapor experiment in order to prevent any moisture backflow. Water was used to collect steam since the amount of moisture backflow is trivial compared to steam supplied in experiment. Silicone oil contaminated by water requires special drying agents to purify for future usage. [72] Therefore, silicon oil was not used in the water vapor involved experiments. All gases were conducted into a hood for lab environment safety.

3.4 Experimental Procedures

3.4.1 Fabrication of SiC Pellets

SiC powders (purchased form Superior Graphite) with 16.9 μm (coarse) and 0.6 μm (fine) nominal particle size were mixed at a 3:2 weight ratio with 10 wt% of SMP-10 (purchased from Starfire Systems Inc.) in a ball miller for 1 h. SMP-10 is an allyl-hydrido-poly-carbo-silane (AHPCS) which yields Si and C elements at a 1:1 molar ratio forming amorphous silicon carbide below 1200 ºC. The slurry was pressed into green pellets (height: 3 mm, diameter: 13 mm) at 600 MPa in a cold uniaxial pressing equipment. The green compacts were then calcinated in an alumina tube furnace up to 1050 ºC with a constant argon (ultra high purity 99.999%) flow. A standard sintering

temperature profile recommended by Starfire Systems Inc. was followed in order to obtain the highest SiC yield, as shown in Figure 3-2. This SiC fabrication method to use pre-ceramic polymer precursor (PPP) has been systematically studied by Chunghao Shih, a member of Dr Baney's group.

3.4.2 Reaction of SiC Powder

Alumina crucibles containing mixtures of SiC powder (purchased from Alfa Aesar, 1 μm) and anhydrous Na_2CO_3 salt (purchased from Alfa Aesar), were placed midway in the tube furnace. The samples were held at 900 ºC for various time, after which they were rapidly quenched in air and then immersed in boiling nanopure water to dissolve the products and residual Na_2CO_3. The unreacted SiC and solution were then transferred to centrifuge tubes, centrifuged, and dried in a vacuum oven. The non-reacted SiC was weighed. The average weight loss percent of three SiC specimens was determined. Blank experiments, in which SiC powder without mixing with salt experienced the same heat treatment and washing procedures, were performed to determine the weight loss of SiC due to the handling error.

3.4.3 Reaction of SiC Pellets

Reaction-bonded SiC (diameter: 5 mm) rods (purchased from Goodfellow Corporation; relative density: 95%) were cut into pellets with a uniform thickness (2 mm). The SiC pellets were mechanically polished using 800-1200 grit discs. Crucibles containing a SiC pellet and Me_2CO_3 salts (Me=Na and K, from Alfa Aesar) were placed midway along the tube furnace. The initial molten salt depth, a distance between the salt/air interface to the upper surface of the SiC pellet, was varied up to 6 mm. All of the SiC samples were confirmed to be totally immersed in molten salts during corrosion

based upon observation after reaction and theoretical calculation of the molten salt depth described below.

$$D = H - h \tag{3-1}$$

$$H = H_0 + H_c \tag{3-2}$$

$$H_0 = \frac{W_s}{A_c \rho_s} \tag{3-3}$$

$$H_c = \frac{V_{SiC}}{A_c} \tag{3-4}$$

Where D is the molten salt depth (mm), H is the height of the salt bath (mm), h is the height of the SiC pellet (mm), H_0 is the height of the salt bath without the SiC pellet (mm), H_c is the height increase of the salt bath with the SiC pellet (mm) compared to the salt without SiC, W_s is the weight of salt (g), A_c is the bottom area of the crucible (mm^2), ρ_s is the salt density at certain temperature. Density of K_2CO_3 and Na_2CO_3 at 1050 ºC is 1.85 g/cm^3 and 1.90 g/cm^3, respectively. [73] V_{SiC} is the volume of the SiC pellet (mm^3). Some parameters were schematically shown in Figure 3-3.

The tube furnace was heated at 900 ºC and 1050 ºC, followed by an isothermal holding up to 15 h. A vacuum was applied at different stages of the corrosion tests as shown in Figure 3-4 in order to remove the reactive gases. UHP Ar gas was supplied at the heating and cooling ramps. The reactive gases were applied at the isothermal holding stage.Different atmospheres (air, Ar/O_2, Ar/CO_2, O_2/CO_2, Ar/H_2O, O_2/H_2O and CO_2/H_2O) with a constant total gas flow were applied in the furnace at the isothermal stage. The partial pressures of O_2, CO_2 and H_2O gases were varied by controlling their flow rates. The total flow rates of the CO_2/H_2O gas mixture were varied in a range of

0.2-1 mol/h. After corrosion, the residues of the SiC pellets were cooled in the Ar gas followed by immersing in nanopure water to remove the salt and the silicate and then drying in a vacuum oven. All corrosion experiments were triplicated in order to obtain the average weight loss percent of SiC pellets under each condition. The sample weight loss percent was calculated using the formula:

$$W_{loss}(\%) = \frac{W_0 - W_a}{W_0} \times 100\% \quad (3\text{-}5)$$

Where W_{loss} (%) is the weight loss percent of the SiC sample, W_0 is the initial weight of the SiC pellet (g) and W_a is the weight of the residual SiC pellet after washing and drying (g).

3.5 Characterization

3.5.1 Particle Size Measurement

The particle size and size distribution of initial SiC powder was characterized using an aerosizer (TSI PSD 3603). This equipment is provided by Particle Engineering Research Center (PERC). The powder sample was milled using mortar and pestle to break the soft aggregations. The measurement was tripled to obtain the average value.

3.5.2 Density Measurement

Density of the synthesized SiC pellets was determined by using the conventional Archimedes's method. The surface of all SiC pellets was first covered by a slight amount of Vaseline in order to prevent water molecules penetrating into the open pores. The weight difference between a SiC pellet with and without Vaseline was less than 1% which can be ignored. After measurement, pellets were immersed in ethanol and cleaned in an ultrasonic bath for 2 min to remove the Vaseline layer. Another density measurement method utilized a caliper to measure height and diameter of a pellet so

that the whole volume can be calculated. The bulk density can be determined from the volume and weight. The density difference measure by both methods is less than 1%. Relative density (RD) of a SiC pellet can be calculated by using the following equation:

$$RD = \frac{\rho_{mea}}{\rho_{ref}} \times 100\% \tag{3-6}$$

$$\rho_{mea} = \frac{W_{SiC}}{V_{SiC}} = \frac{4W_{SiC}}{\pi d^2 h} \tag{3-7}$$

Where RD is relative density, ρ_{mea} is the density of the SiC pellet being measured, ρ_{ref} is the density of the reference which is 3.21 g/cm^3, W_{SiC} is the weight of the SiC pellet and d and h are the diameter and height of the SiC sample, respectively, which can be determined by using a caliper.

3.5.3 Profilometer

A wyko optical profilometer (Wyko NT1000) was used to measure the surface area index (SAI) of SiC samples after polishing in order to assure that the surface area of polished SiC samples are approximately identical. SAI can be calculated through the following equation:

$$Surface\ Area\ Index\ (SAI) = \frac{Surface\ Area\ (SA)}{Lateral\ Surface\ Area\ (LSA)} \tag{3-8}$$

In which, surface area is the total exposed three-dimensional surface area being analyzed, including peaks and valleys. The lateral surface area is the surface area measured in the lateral direction. The surface area index is a measure of the relative flatness of a surface. An index which is approximate to unity indicates a very flat surface where the lateral (XY) area is very close to the total three-dimensional (XYZ) area. Since the LSA in the field of view is in 0.1 mm^2 scale which is much less than the

dimension of SiC samples, the SAI of 20 different sites of each sample were collected to obtain the average value.

3.5.4 X-ray Diffraction (XRD)

The product was crushed into fine powder by using an alumina mortar and pestle. An X-ray Diffraction Philips APD 3720 was used to identify the corrosion product. Data was collected from a 2θ angle of 10º to 130º. The operation voltage and current were set to 45 KV and 40 mA. Copper Kα radiation was used in measurement.

3.5.5 Scanning Electron Spectroscopy (SEM)

The microstructure of the synthesized SiC pellets prepared by calcinating pre-ceramic polymer precursor was characterized using scanning electron spectroscopy (SEM, JEOL 6335F). Pellets were cut with a diamond saw. The cross section of the pellets was mechanically polished using diamond paste of different particle size from 15 to 1 μm. The cut surface of pellets was then cleaned in ethanol in an ultrasonic bath for 2 min.

Elements of the corrosion products were identified using Energy dispersive X-ray spectroscopy (EDS) which is connected with SEM. The dry products were crushed into fine powder using a mortar and postal. The powder was then mounted in an epoxy substrate followed by polishing using 800-grit SiC discs. All samples prepared for SEM and EDS examination were sputter-coated with a carbon thin film. The SEM was operated with an accelerating voltage of 15 kV and a working distance of 15 mm.

3.5.6 Transmission Electron Spectroscopy (TEM)

The morphology of reacted SiC powder was examined using transmission electron spectroscopy (JOEL 200CX) operated at 200 keV. The residual SiC powder collected after the molten salt reaction process was suspended in ethanol through ultrasonication

for 5 min. A droplet of the dispersion solution was transferred onto a cooper grid for analysis.

3.5.7 Inductive Coupled Plasma Spectroscopy (ICP)

Potassium (K), silicon (Si) and cerium (Ce) concentrations in different washing solutions were determined using inductive coupled plasma spectroscopy (Perkin-Elmer Plasma 3200). The commercial standard solutions for each element were diluted in nanopure water. The solutions which contained 0.1 ppm, 1 ppm, 10 ppm and 100 ppm target elements were prepared according to a standard procedure. The measurement for each element was replicated by five times.

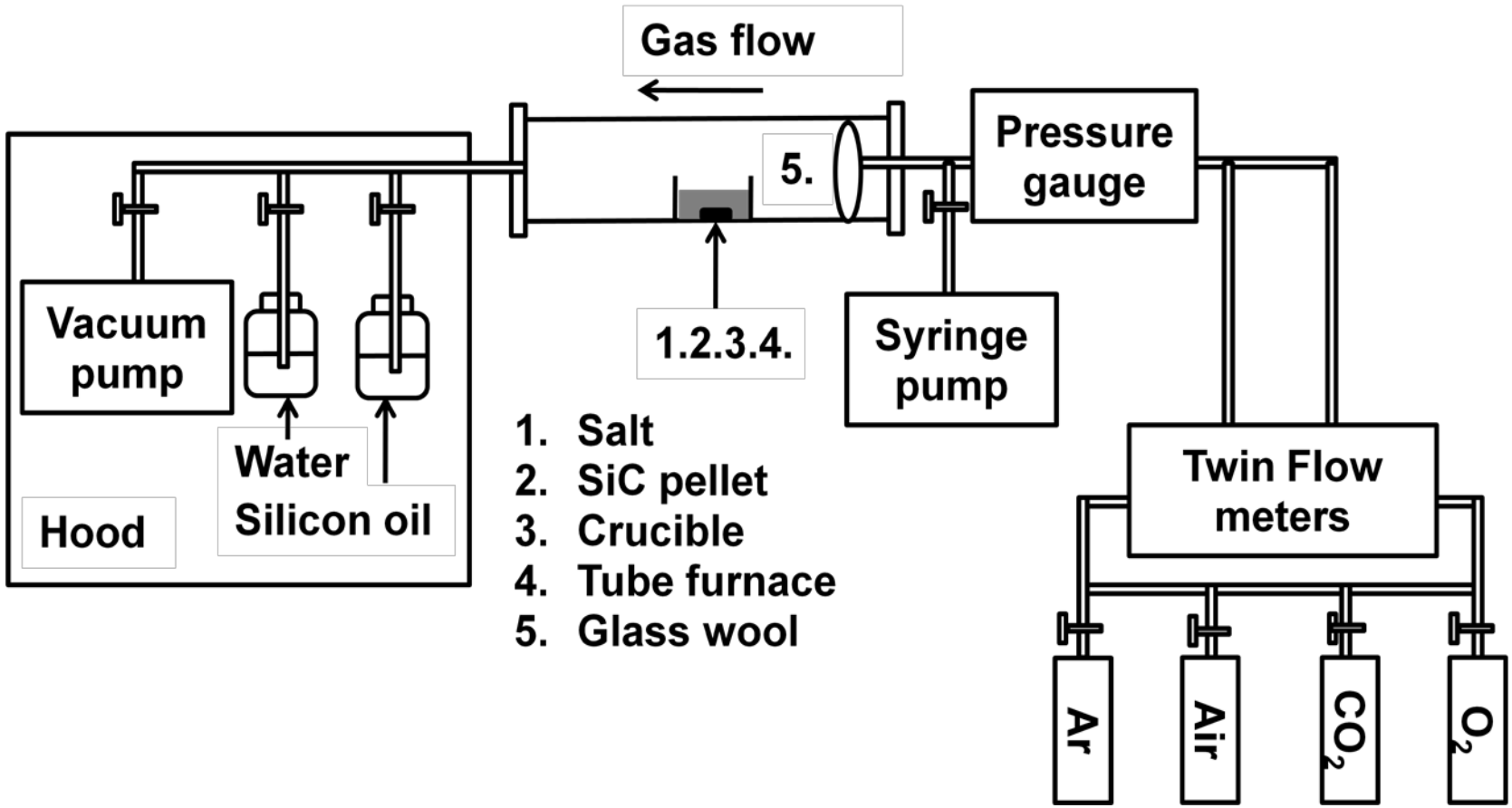

Figure 3-1. Schematic of process design

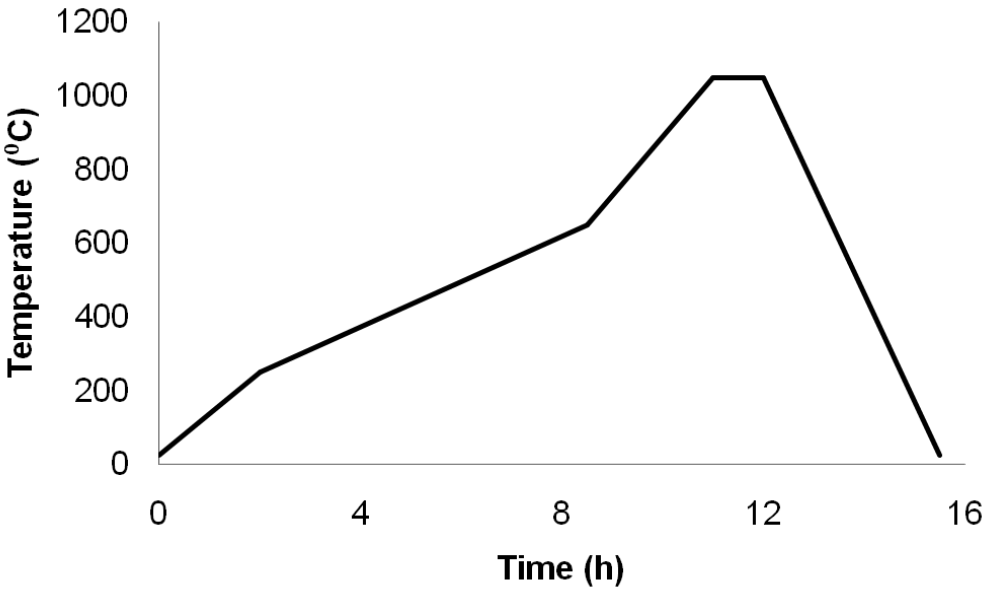

Figure 3-2. Schematic of heating profile for synthesis of SiC pellets

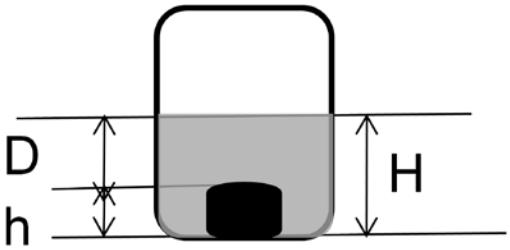

Figure 3-3. Scheme of molten salt depth (oxygen diffusion distance) in a crucible

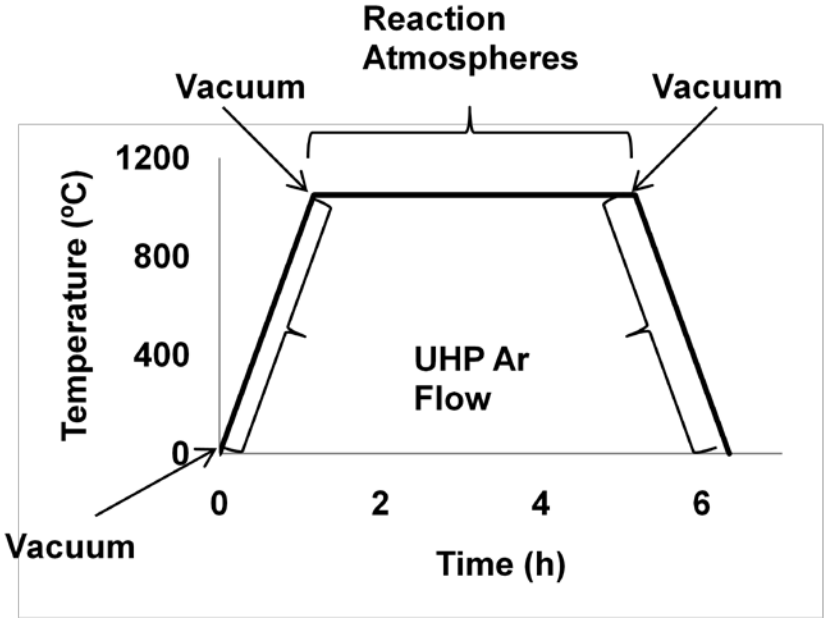

Figure 3-4. Heating and atmosphere profile of the corrosion experiment

Table 3-1. Elevation of the molten salt candidates and their properties

Salt	Melting point (ºC)	Decomposition point (ºC)	Gas products	Boiling point (ºC)	Evaluation
Na_2CO_3	851	890	CO_2	1600	Good
$NaHCO_3$	270	270	CO_2, H_2O	1600	Unstable
Na_2SO_4	884	1100	SO_2, SO	1429	Corrosive gas
$NaHSO_4$	315	315	SO_3	1429	Corrosive gas
$NaNO_3$	308	600	O_2, NO	380	Low boiling point
NaCl	801	N/A	Cl_2	1413	Low reaction rate
NaOCl	18	101	O_2, Cl_2	101	Low boiling point
$NaClO_3$	248	300	O_2	300	Low boiling point
NaF	993	N/A	N/A	1695	No reaction with SiC
Na_3PO_4	600	N/A	N/A	N/A	No reaction with SiC
NaOH	318	N/A	N/A	1388	Handling difficulty
K_2CO_3	891	891	CO_2	N/A	Good
$KHCO_3$	292	292	CO_2, H_2O	N/A	Unstable
K_2SO_4	1069	1689	SO_2, SO	1689	Corrosive gas
$KHSO_4$	197	300	SO_3, SO_2	N/A	Corrosive gas
KNO_3	334	400	O_2, NO	400	Low boiling point
KCl	770	N/A	N/A	1420	Low reaction rate
$KClO_3$	356	400	O_2	400	Low boiling point
KF	858	N/A	N/A	1505	No reaction with SiC
K_3PO_4	1384	N/A	N/A	N/A	High melting point
KOH	360	N/A	N/A	1327	Handling difficulty

CHAPTER 4
THE EFFECTS OF SALT TYPE, SALT AMOUNT, SALT DEPTH AND REACTION TIME

4.1 Introduction

Silicon carbide specimens without ceria were tested in order to build a baseline for this reprocessing method. The SiC/salt reaction mechanism was introduced. SiC fine powder with a large surface area was used to test the feasibility of the molten salt reaction/dissolution method. The reaction kinetics of bulk SiC was then studied. The effects of salt type, depth of the molten salt and the salt to SiC molar ratio on the reaction kinetics are discussed in this chapter.

4.2 Basic Mechanisms of the Reprocessing Strategy

In an oxidizing atmosphere, SiC is covered by a thin silica layer which protects it from further oxidation. The silica layer can react with the molten carbonates to form crystalline or molten silicates depending on the reaction temperature. The formed silicates, either solid or liquid, have lower density than silica which allows further oxidation and corrosion of SiC. It has been reported that oxygen diffusivity in amorphous silica and in a sodium silicate is approximately 10^{-15} cm^2/s and 10^{-9} cm^2/s, respectively, at 1000 ºC. [14] This process can be expressed by the following generalized reactions (Q= O_2, CO_2, H_2O; P = CO, H_2 or other gaseous species; M = Na, K):

$$SiC(s) + Q(g) \rightarrow SiO_2(s) + P(g) \quad (4\text{-}1)$$

$$M_2CO_3(l) + SiO_2(s) \rightarrow M_2SiO_3(s) + CO_2(g) \quad (4\text{-}2)$$

The molten salts decompose above their melting points:

$$M_2CO_3(l) \rightarrow M_2O(l) + CO_2(g) \quad (4\text{-}3)$$

The generated metal oxides (M_2O) usually have high vapor pressure. [74] Therefore, they can easily vaporize at high temperature especially in a flowing gas.

Most of the molten salt/SiC reaction studies have been performed by coating the SiC samples with a thin layer of alkali salts, followed by heating the specimens to desired temperatures. However, the rate-controlling step of this process is not clear up to now due to its complexity in nature. In general, several possible rate-limiting steps which have been proposed include:

1. Diffusion of oxidizing gases through the molten salts,
2. Silica formation (SiC oxidation),
3. The molten salt ions transport to the sample surface,
4. Alkali silicate formation,
5. Outward diffusion of gaseous products such as CO, CO_2 and H_2 through the molten salts to the gas phase.

The mechanism is more complicated if the temperature effect on the silicate product is considered. The silicates can dissolve in the molten salt above their melting temperatures. Diffusion of the silicate ions should be counted as a result. On the other hand, the silicates will leave as a solid layer between the silica film and the salts below their melting temperatures. The diffusion of oxidizers and salt ions through this layer should also be considered. Those mechanisms are demonstrated in Figure 4-1. The investigation on the rate-control step of this molten salt reaction process has practical significances since the IMF reprocessing rate can be adjusted by controlling the rate-limiting step.

Removal of the formed silicates in water is another critical step in order to filter out the non-transmuted fuels. The alkali silicates such as Na_2O-SiO_2 and K_2O-SiO_2 exhibit

high solubility in water. In addition to their crystalline form, alkali silicates also exist in the form of alkali silicate glass with variable SiO_2/alkali oxide ratios, which can be produced by a rapid cooling of silicate melts. Water glass, which is a concentrated solution of the alkali silicates in water can be produced by dissolving silicates in hot water. SiO_2 is found mainly in the form of $(SiO_4)^{4-}$ monomers in the water glass solution. It also exists in larger units, such as $(Si_2O_7)^{6-}$ or $(Si_3O_{10})^{8-}$ chains and $(Si_3O_9)^{6-}$ or $(Si_4O_{12})^{8-}$ rings. [75-76] The degree of polycondensation increases with declining Me_2O/SiO_2 ratio of alkali silicates (Me=Li, Na, K).

The solubility of alkali silicates which have the composition $Me_2O{\bullet}mSiO_2$ depends on the molar ratio (m) between the silica and alkali oxides. [77] For example, sodium orthosilicate (Na_4SiO_4, m=0.5) containing the maximum amount of Na_2O and sodium metasilicate (Na_2SiO_3, m=1) are soluble in cold water (15-25 ºC), while sodium disilicate ($Na_2Si_2O_5$, m=2) is soluble in hot water (90-100 ºC). A silicate with silica content higher than 80% is soluble in water superheated to 120 ºC or higher [39]. As a trend, dissolution of silicates with higher silica content requires higher temperature. To achieve a high solubility of silicate in water, the starting molar ratio of alkali salt e.g. Na_2CO_3 to SiC should be no less than 1 to form the silicate with m equal to or less than 1.

The dissolution process of alkali silicates is complex. It is primarily hydration of silicate with formation of MeOH. For example, sodium orthosilicate and sodium metasilicate hydrolyze in an aqueous solution according to the following reaction:

$$Na_4SiO_4 + H_2O \rightarrow 2NaOH + Na_2SiO_3 \quad (4\text{-}4)$$

$$Na_2SiO_3 + H_2O \rightarrow NaHSiO_3 + NaOH \quad (4\text{-}5)$$

Potassium silicates are more soluble in water compared to sodium silicates at a given molar ratio of silica and alkali oxide. Since sodium is more electro-negative than potassium, the ionic bonds of potassium silicate are more easily broken by water molecules.

4.3 Result and Discussion

4.3.1 Characterization of Initial SiC Powder

As shown in Figure 4-2, the initial SiC powder has a bimodal particle size distribution on the volume percent curve. Most particles form big agglomerations which have a particle size larger than 10 μm. Figure 4-3 shows the XRD profile for the initial SiC powder (1 μm). This result verified that the starting SiC powder is the β phase.

4.3.2 Reaction of SiC Powder

4.3.2.1 Starting materials with sufficient mixing

The weight loss percentage of SiC powder (1 μm) vs. time is shown in Figure 4-4, in which complete SiC powder 1 μm dissolution in Na_2CO_3 molten salt were achieved in 0.5 h at 900 ºC. The average weight loss due to handling error on 1 μm SiC powder was less than 1%. Under the same condition, this result is a negligible operation error. For both SiC specimens, the corrosion product sodium metasilicate Na_2SiO_3 in Na_2CO_3 salt was identified by an X-ray diffraction study as shown in Figure 4-5.

4.3.2.2 Starting materials without sufficient mixing

Mixing the starting powder with salt significantly affects the reaction rate of powder SiC. The initial samples without mixing showed a slower reaction rate compared to the rate of the well mixed sample. The reaction terminated after approximately 2 h. Figure 4-6 shows the SiC sample weight loss as a function of time. In the first 2 h, the SiC weight loss rate is significant. However, no further weight loss occurs after 2 h. The SiC

powder weight loss after 6 h reaction is similar to the value obtained in 2 h which is approximately 76%. A higher reaction rate was found when mixing the starting materials in a ball miller for 10 min, as shown in Figure 4-7. The reaction terminated when 90% SiC dissolution was achieved. This phenomenon may be because the fine SiC powder tends to cluster in the melt to reduce the surface energy and settle down on the bottom of the crucible. The oxygen concentration at the bottom may be too low to achieve a rapid oxidation of SiC. Another possible explanation is that the SiC powder size increases due to clustering, hence molten salt ions may not pass through the thick silicate layer produced on the SiC particle surface. Corrosion would be terminated as a consequence. A cluster of the SiC particles after reaction with the molten salt was verified by TEM examination, as shown in Figure 4-8. Therefore, a higher reaction rate and complete dissolution could be achieved by homogenously mixing the SiC powder and the salt.

4.3.3 Reaction of SiC Pellets

Based on the promising results obtained in the powder work, further study was conducted to dissolve monolithic pellets of SiC in Na_2CO_3. The weight loss of SiC pellets was found to be very low under the same experiment conditions as the powder dissolution, even at an elevated temperature e.g. 900-1050 ºC up to 15 h. A number of reports postulated that the formed silicates retarded the ion transportation to explain this phenomenon. [13, 59-64] Since the crystalline silicates were formed at the interface between SiO_2 and the molten salt, the continuation of the reaction requires mobile sodium ions to transport across the increasing layer of crystalline sodium silicates. The amount of molecules and ions diffusing through the interface would decrease as the silicate layer increases. Once the silicate layer grows to a critical thickness, molten salt

ions may not pass through the thick silicate layer and result in SiC dissolution. Corrosion will be terminated as a consequence.

Two methods can be considered to prevent termination of the SiC recession:

1. Grinding bulk SiC into micron-size powder which results in total consumption of SiC before formed silicates reach a critical layer thickness.
2. Removing the silicate layer from SiC pellets by dissolving it in the molten salts above the melting temperature of silicates.

The first method is not desirable in the nuclear industry due to the potential radiological contamination. The second method was selected, since this method can be applied on a large scale. Crystalline sodium silicate in hot corrosion has a melting temperature at 1090 ºC. In comparison, if potassium carbonate instead of sodium carbonate is used as the molten salt for SiC corrosion, the formed potassium silicate has a melting temperature of 977 ºC. Therefore, the K_2CO_3 salt was selected.

The average surface area index (SAI) of each RB-SiC pellet after polishing used in these experiments was measured in a range of 1.2 $\pm$ 0.05 using the optical profilometer. The surface area of samples was kept nearly constant in order to minimize its effect on the corrosion rate. All of the SiC samples were confirmed to be totally immersed in molten salts during corrosion based upon observation after corrosion and theoretical calculation of the molten salt depth described in Chapter 3.

The corrosion temperature for the bulk SiC was increased to 1050 ºC in order to assure the melting of the potassium silicate layer formed on the SiC surface. A significant SiC sample weight loss of about 20% was found in an experiment in which an 8 mm RB-SiC rod was corroded in the K_2CO_3 molten salt at 1050 ºC for 8 h. An interesting phenomenon was observed that a flat surface facing towards the air was

created on the SiC rod. The crossection of the SiC rod before and after corrosion is shown in Figure 4-9.

The faster corrosion rate of the upper part of SiC rod than the bottom can be explained by a hypothesis that diffusion of oxygen in the K_2CO_3 molten salt controls SiC corrosion rate at 1050 ºC. Solubility and diffusivity of the oxygen in the molten salt system affect the rate of SiC oxidation, as is predicted in the Fick's first law of diffusion:

$$J = - D(\Delta C/\Delta x) \quad (4\text{-}6)$$

where, J is the oxygen flux approaching to SiC surface, ΔC is the oxygen concentration at the gas/molten salt interface, which depends on the solubility of oxygen in the molten salt, assuming that the oxygen concentration at the SiC/molten salt interface is equal to zero due to immediate SiC/oxygen reaction, Δx is the oxygen diffusion distance from the gas/molten salt interface to the SiC/ molten salt interface and D is the oxygen diffusion coefficient. The oxygen flux increases with a decreasing oxygen diffusion distance, an increasing diffusion coefficient and an increasing solubility of the oxygen which largely depends upon the partial pressure of oxygen in the gas phase.

Maru et al. [78-79] summarized that the solubility of oxygen within a temperature range of 600 ºC to 800 ºC in molten carbonates is controlled by the reactions with the melt to generate peroxide (O_2^{2-}), superoxide (O^{2-}) ions and carbonate dioxide (CO_2). The solubility of oxygen in the molten carbonates will be enhanced with a decreasing partial pressure of CO_2 since CO_2 is a product in the O_2/carbonate reaction. In other words, the presence of the CO_2 in the gas atmosphere would be a negative factor to SiC corrosion. However, CO_2 can also act as an oxidizer to SiC, which increases the complexity of the mechanism of SiC corrosion. The effect of those factors on the SiC

corrosion rate will be discussed in chapter 4. Systematic data were collected in the following experiment to study if the oxygen diffusion distance affects the SiC corrosion rate.

4.3.3.1 Salt amount

The reprocessing strategy reported in this work is based on formation of the water soluble silicates from which ceria can be filtered out. It has been discussed that water solubility of the alkali silicates which has the composition $Me_2O•mSiO_2$ (Me= Na, K) highly depends on the salt to SiC molar ratio. To achieve a high solubility of silicates in water, starting molar ratio salt to SiC would have to be no less than 1 to form silicate with m equal to or less than 1. Therefore, the initial salt to SiC molar ratio applied in this work were all higher than 1.

Since a change of the salt depth in the crucibles results in varying the salt amount, it is necessary to study if the salt amount would affect the corrosion rate before examining the effect of the molten salt depth, given the sufficient amount of salt to produce water soluble silicates. Three crucibles A, B and C with various sizes contained the salts with the same depth (4 mm) but at different molar ratios to SiC, as illustrated in Figure 4-10. Crucible A had a cylinder shape with 21 mm diameter and 30 mm height; Crucible B had a rectangular shape with 50 mm length, 35 mm width and 20 mm height; Crucible C had a rectangular shape with 75 mm length, 35 mm width and 20 mm height.

After corrosion at 1050 ºC for 1 h, the SiC pellets placed in three crucibles showed a similar weight loss in the molten K_2CO_3 salt or Na_2CO_3 salt as shown in Figure 4-11. However, the SiC weight loss under the same corrosion condition in three crucibles was found to be unequal when the corrosion time was extended to 3 h. This result may be attributed to the molten salt depths in those crucibles reducing at different rates with

extended reaction time. Calculated values of molten salt depth shown in this work represented the depth at the beginning of the corrosion process. Alkali carbonates volatized and decomposed at 1050 ºC [18], which would result in reducing the salt depth. This result demonstrated that given an excess of salt, the salt to SiC molar ratio had little effect on the rate of corrosion when the salt depth was unchanged. Therefore, the isothermal holding time was limited in 1 h in the experiment of the molten salt depth to minimize the salt loss due to vaporization. As observed in Figure 4-11, SiC pellets dissolved faster in molten K_2CO_3 salt than in Na_2CO_3 at 1050 ºC. It has been reported that the vapor pressure of Na_2CO_3 and K_2CO_3 at 1050 ºC is approximately 2500 Pa and 500 Pa. [98] The salt depth of Na_2CO_3 should decrease faster compared to K_2CO_3, because Na_2CO_3 has higher volatility rates than K_2CO_3, which should accelerate the corrosion as a consequence. However, it was not observed experimentally. This result was consistent with the early hypothesis that potassium silicate melting enhanced SiC corrosion in K_2CO_3 salt at 1050 ºC.

4.3.3.2 Molten salt depth

In order to investigate whether the rate of SiC corrosion in molten carbonate salts at 1050 ºC was affected by the oxygen diffusion distance in the salt, various molten salt depths of K_2CO_3 and Na_2CO_3 salt were examined. The salt depth utilized in experiment was maintained at no less than 2 mm in order to assure that SiC pellets were completely immersed in the molten salts during the corrosion. An increasing SiC dissolution rate was observed, as expected, with a decreasing depth of the molten salt K_2CO_3 and Na_2CO_3 salt at 1050 ºC, as shown in Figure 4-12. A higher corrosion rate in K_2CO_3, than in Na_2CO_3, was found of all molten salt depths. This result reinforced the

hypothesis that oxygen diffusion may affect SiC corrosion in the molten alkali carbonates.

4.3.3.3 Reaction time

The factor of reaction time was studied to examine the reaction behavior of bulk SiC in extensive time. Figure 4-13 shows the weight loss percent of the SiC samples as a function of reaction time. The average weight loss percent of three SiC specimens follows a linear trend as an increase in reaction time. This result implied a constant reaction rate of bulk SiC in the molten salts. As discussed in chapter 3, the oxidation of SiC in air exhibits parabolic kinetics. The reaction is controlled by oxygen diffusion in the silica layer which progressively grows as time increase. In the molten salt environment, the oxidation is accelerated because of silica dissolution in a form of a silicate liquid or transformation into a low density silicate, which enhances the oxidizing gases diffusion to the interface of SiC/salt. Moreover, the oxygen diffusion distance is steadily reduced during reaction due to dramatic salt volatilization above the decomposition temperature of the carbonates. For Na_2CO_3 and K_2CO_3, the melting temperatures are equal to the decomposition temperature. The previously presented results confirmed that reducing the molten salt depth decreased the oxygen diffusion distance, which consequently increases the SiC dissolution rate in the molten K_2CO_3 and Na_2CO_3 salts at 1050 ºC. However, the total interface area of SiC/molten salt was continuously decreased due to reaction which resulted into the reaction deceleration. The constant reaction rate during extensive time period may be attributed to a counterbalance of the effect of the total surface area of the SiC specimen and the oxygen diffusion distance controlled by the salt evaporation rate.

After washing the residues of SiC and the K_2CO_3 salt in boiling water, a large amount of white precipitates were found in the washing solution. The precipitates were centrifuged and separated from the solution for XRD and EDS examination. The stochiometric composition of the precipitate labeled as A consisted of K, Si, Al and O, as shown in Table 4-1. These results indicated that the alumina crucibles which were attacked by the the molten salt partially dissolved in the K_2O-SiO_2 melt. Two crystalline phases Kalsilite ($KAlSiO_4$) and Leucite ($KAlSi_2O_6$) and an amorphous phase were detected in the precipitate by using XRD, as shown in Figure 4-14. However, the crystalline phases disappeared when the reaction time was shortened to 4 h. The XRD pattern of the product obtained after corrosion for 4 h was shown in Figure 4-15. As shown in Table 4-1, this product labeled as B was also composed of K, Si, Al and O. The crystalline phase formation in the melt requires sufficient time for ions and molecules diffusing, which explained no detectable crystalline phase in the precipitate obtained in the 4 h reaction. [80] The lower stoichiometric concentration of K_2O in the precipitate obtained in 8 h may be due to the dramatic K_2O volatilization at 1050 ºC. [74]

The K_2O-SiO_2-Al_2O_3 precipitates did not dissolve in boiling water for extensive time. The precipitate B was totally dissolved in the 50% KOH solution within 1 min at 80 ºC with stirring. The precipitate A with the same amount required at least 10 min to dissolve completely in the 50% KOH solution. It has been known that alumina which can act as an acid is able to dissolve in potassium hydroxide solution yielding aluminates:

$$Al_2O_3(s) + 2KOH(l) = 2KAlO_2(l) + H_2O(l) \quad (4\text{-}7)$$

The aluminates exists in the basic solution in a form of aluminate ions such as AlO_2^- or $Al(OH)_4^-$. [81]

Moreover, silica can dissolve in KOH solution yielding silicates:

$SiO_2(s) + 2KOH(l) = K_2SiO_3(l) + H_2O(l)$ (4-8)

Amorphous silica and alumina have been found to dissolve more rapidly in the basic solution than their crystalline phases since the amorphous phase has more open space for the basic ions penetrating and more dangling bonds leading to a high reactivity. [82] Silicon was also detected in the washing solution using ICP, whereas no Al was found in the solution which indicated that in K_2CO_3 salt SiC was transformed into the water soluble silicates and non-water soluble alumino-silicates at 1050 ºC. After washing the SiC residues and Na_2CO_3 salt in hot water, no precipitates was generated. Sodium silicate (Na_2SiO_3) was detected after drying the washing solution. This result may be because the formed Na_2SiO_3 on SiC surface did not dissolve in the molten salt at 1050 ºC. Therefore, the Na_2O-SiO_2-Al_2O_3 phase was not generated.

4.4 Conclusions

Complete reaction of fine SiC powder with the molten salt at 900 ºC indicated the feasibility of this reprocessing method proposed in this work. The strategy was further tested on bulk SiC for the practical needs. However, a higher processing temperature and a more efficient salt were required to completely dissolve the bulk SiC specimens in a limited time. Understanding the mechanism of this process is critical because the processing condition can be optimized by manipulating the rate-controlling step. However, SiC/molten salt reaction is very complex, which involves SiC oxidation, salt ion diffusion, silicate formation and dissolution and gas inward and outward diffusion. Compare to the Na_2CO_3 salt, the reprocessing can be performed at a comparatively lower temperature in the K_2CO_3 salt due to the lower melting points of the potassium silicates. The SiC/molten salt reaction rate at 1050 ºC can be enhanced by decreasing

the molten salt depth, which indicated that the oxygen diffusion in the salt may be the rate-limiting factor of this process.

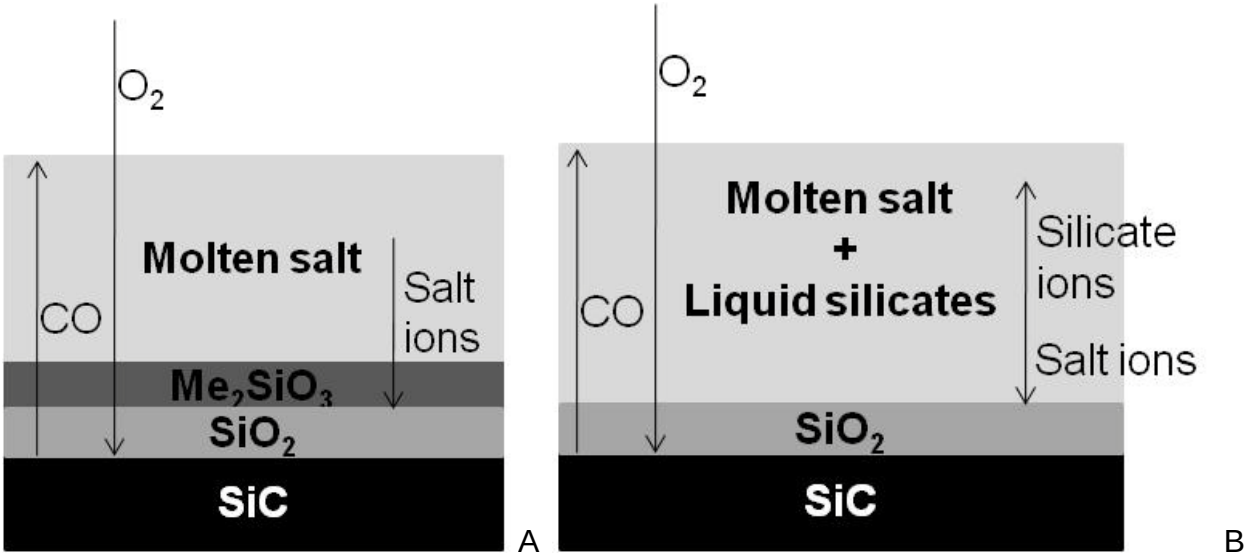

Figure 4-1. Schematic of SiC/salt reaction (Me= Na, K) under O_2 atmosphere A) below the silicate melting temperature B) above the silicate melting temperature

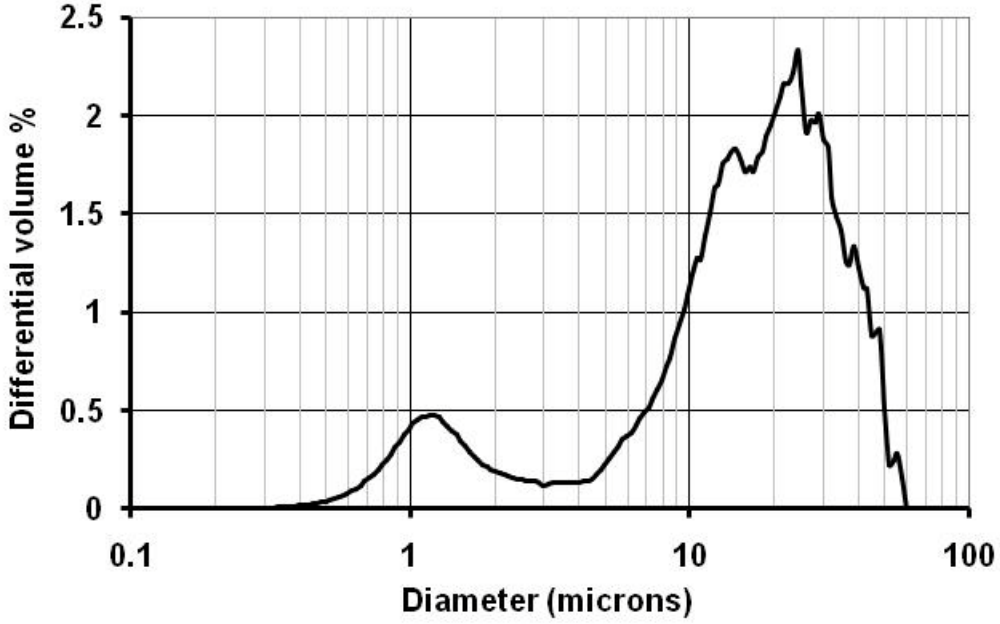

Figure 4-2. Particle size distribution of the initial SiC powder (1 μm) determined by aerosizer

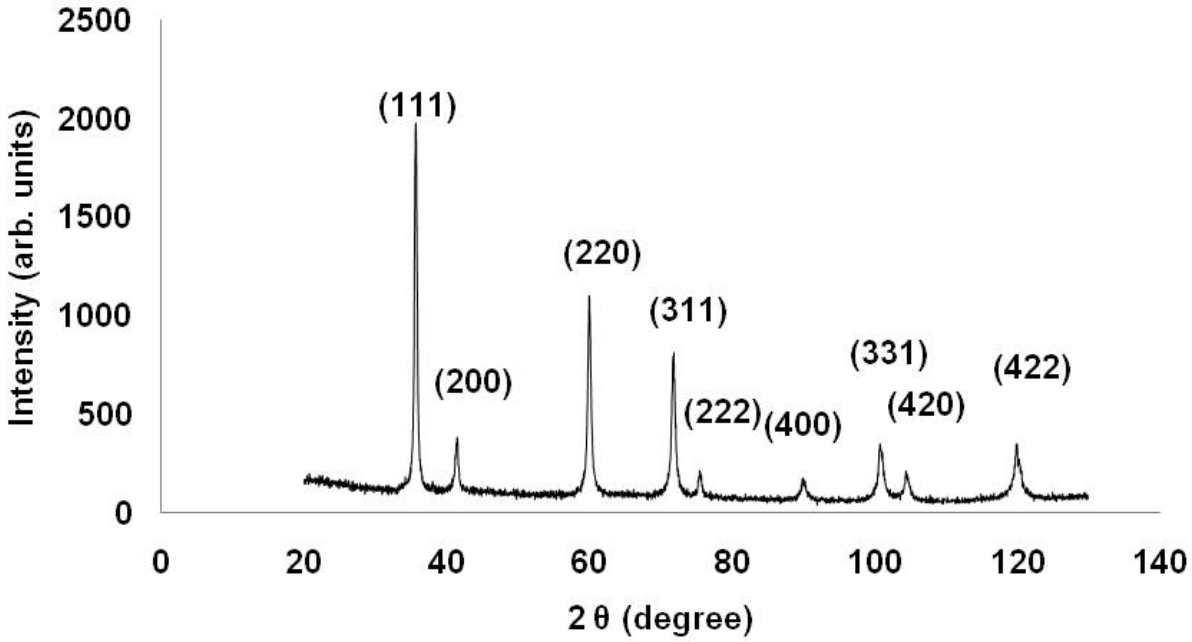

Figure 4-3. XRD profile of the initial SiC powder (1 μm, β phase)

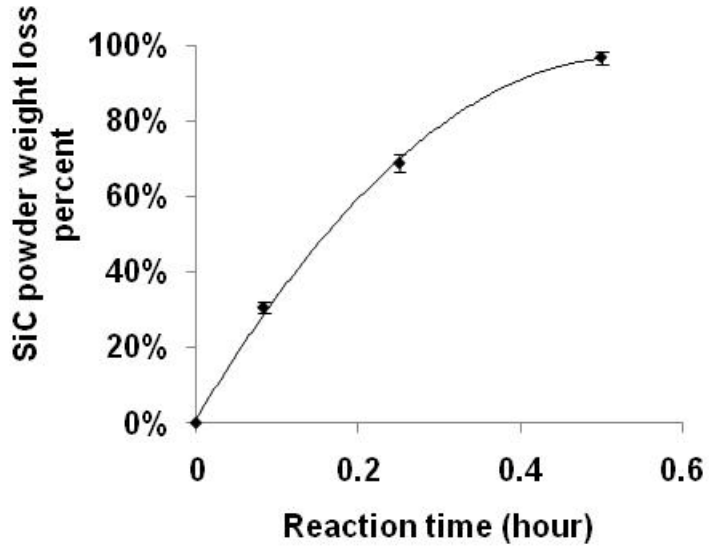

Figure 4-4. Weight loss percent of powder SiC corroded in the molten Na_2CO_3 salt at 900 ºC as a function of reaction time (The SiC powder and salt were homogenously mixed in a ball miller for 1 h.)

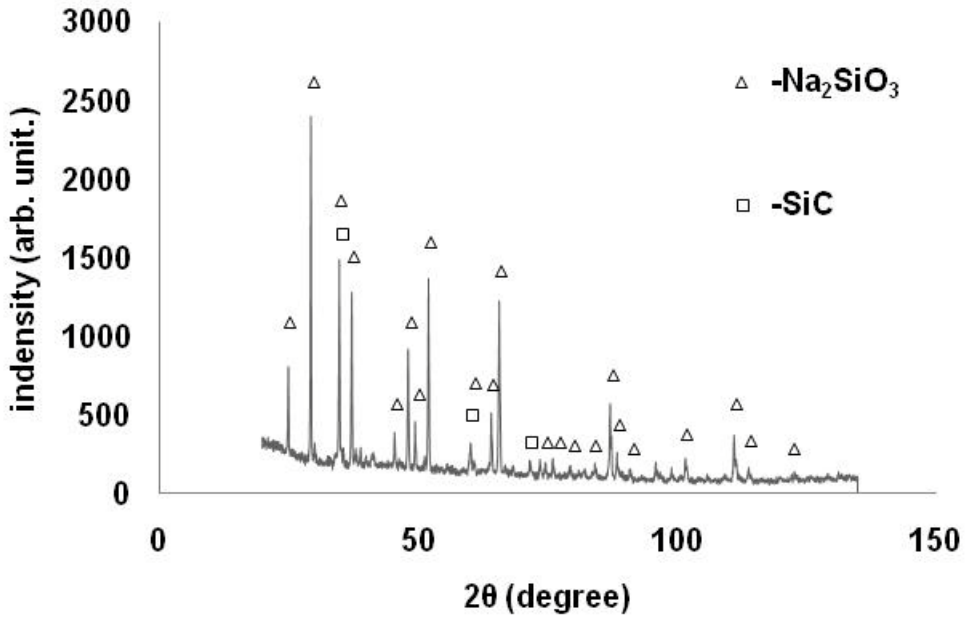

Figure 4-5. XRD profile of the product of SiC/salt reaction at 900 ºC

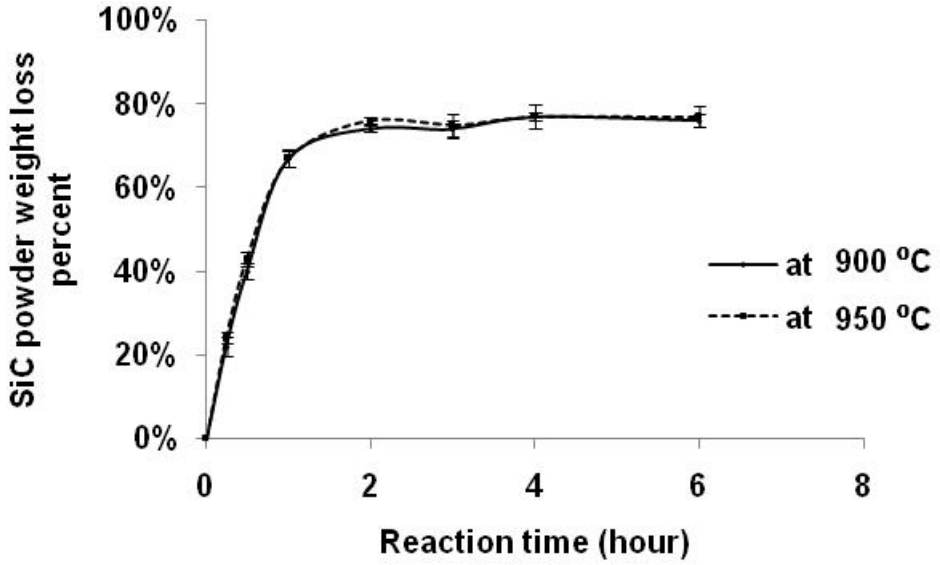

Figure 4-6. SiC powder (1 μm) weight loss percent as a function of reaction time at 900 ºC and 950 ºC (The SiC powder was not mixed with Na_2CO_3 salt.)

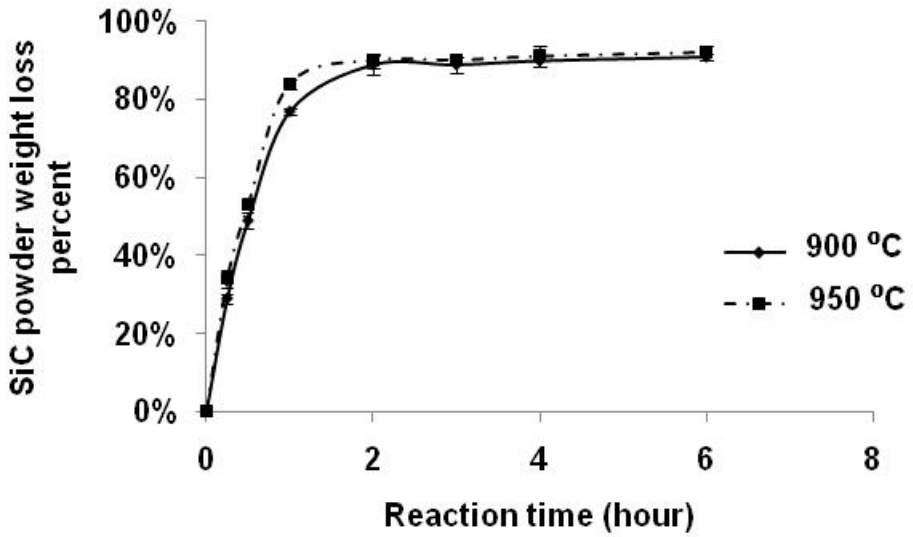

Figure 4-7. SiC powder (1 μm) weight loss percent as a function of reaction time at 900 ºC and 950 ºC (The SiC powder was mixed with Na_2CO_3 salt in a ball miller for 10 min.)

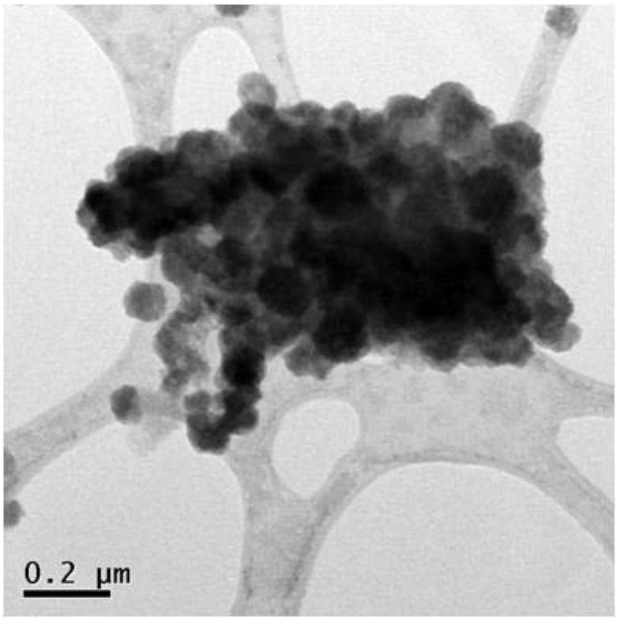

Figure 4-8. TEM image of a SiC cluster

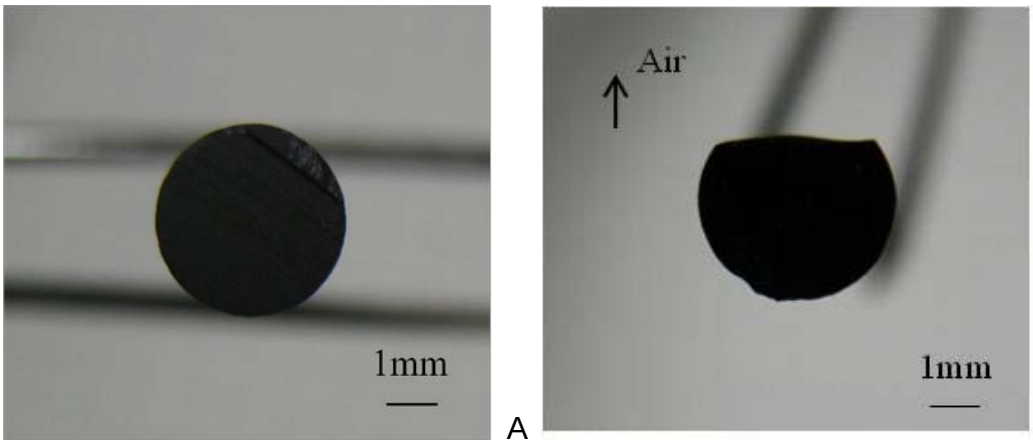

A B

Figure 4-9. The crossection of the SiC rod (a) before corrosion and (b) after 8 h corrosion in the K_2CO_3 molten salt at 1050 ºC

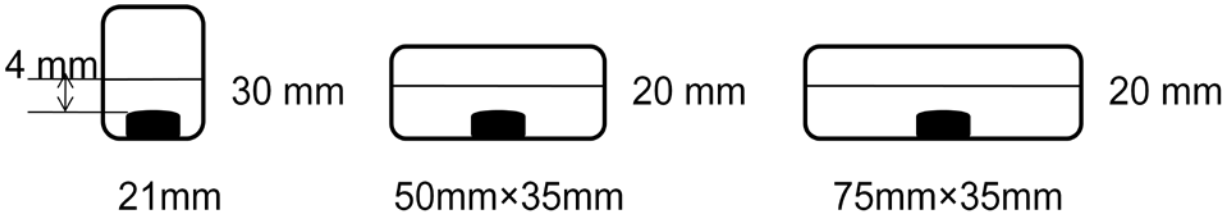

Figure 4-10. Diagram of three crucibles with different dimension but identical salt depth (4 mm)

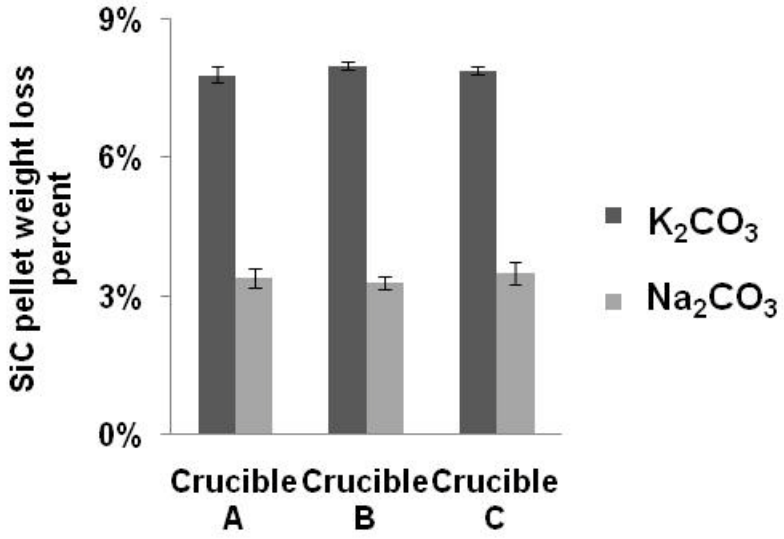

Figure 4-11. Weight loss of SiC pellets corroded at 1050 ºC for 1 h in molten K_2CO_3 and Na_2CO_3 salt, contained in three crucibles with different dimension

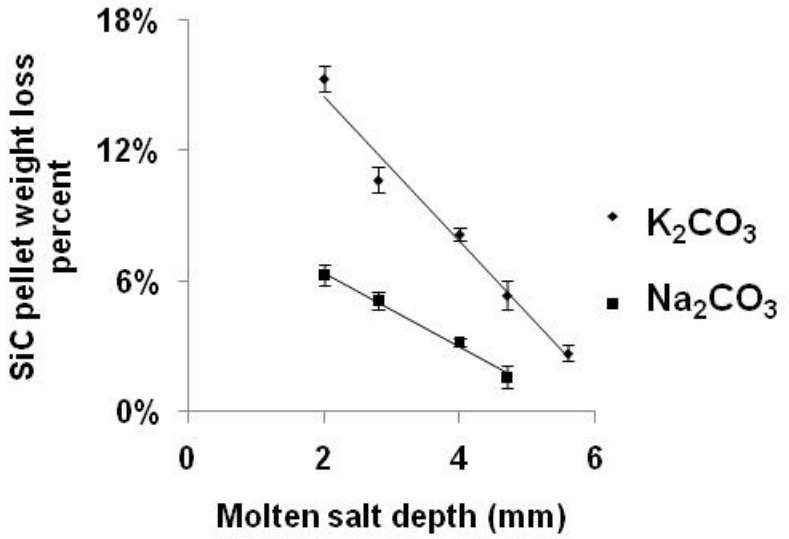

Figure 4-12. Weight loss of reaction-bonded SiC pellets corroded in the molten K_2CO_3 and Na_2CO_3 salts at 1050 ºC for 1 h, as a function of the salt depth

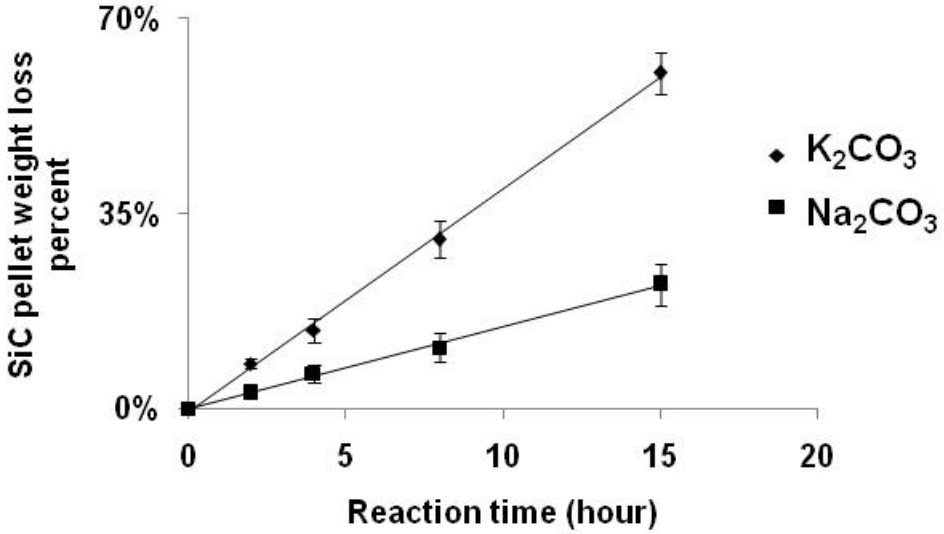

Figure 4-13. Weight loss of reaction-bonded SiC pellets corroded in molten K_2CO_3 at 1050 ºC as a function of the reaction time

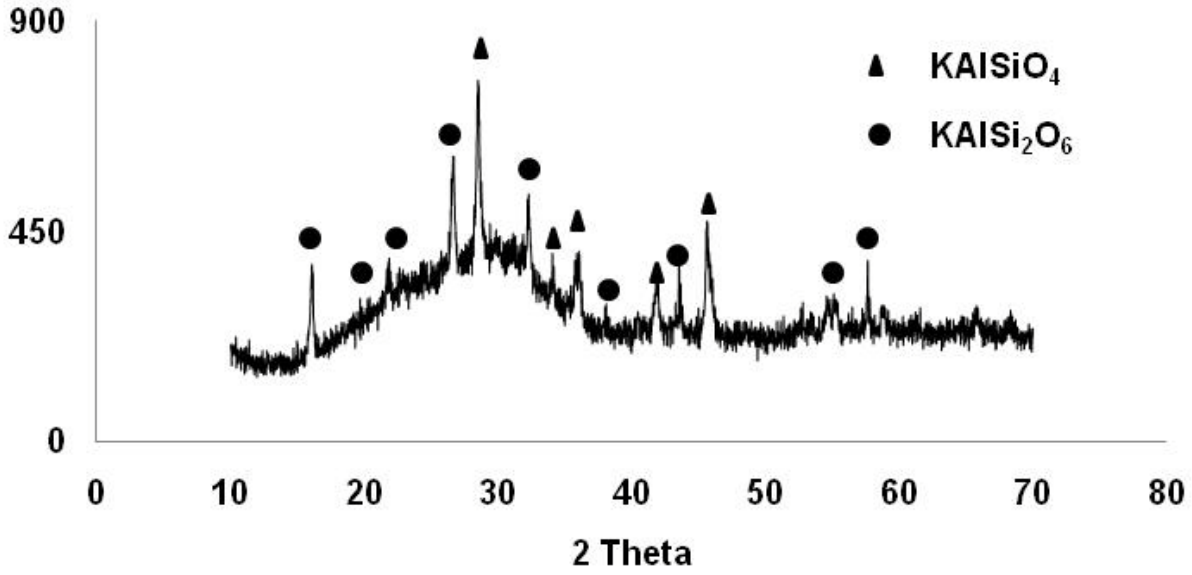

Figure 4-14. XRD spectrum of the precipitate obtained in 8 h reaction

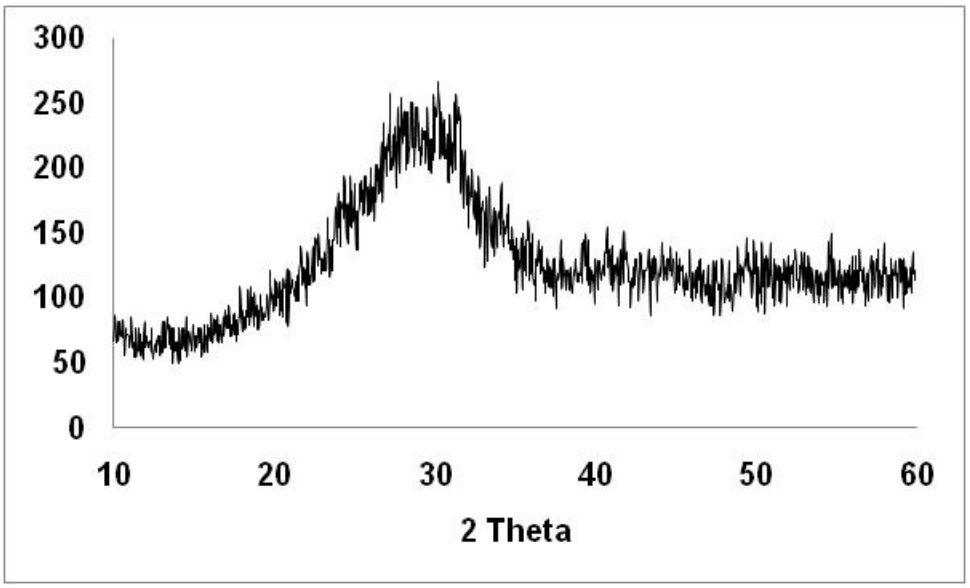

Figure 4-15. XRD spectrum of the precipitate obtained in 4 h reaction

Table 4-1. Composition of the precipitates generated from the SiC/salt reaction at 1050 ºC for 4 h and 8 h

Precipitate	Chemical analysis (atomic %)				Stoichiometry		
	K	Si	Al	O	K_2O	SiO_2	Al_2O_3
A	13.9	16.6	11.0	58.5	1.3	3.0	1
B	27.2	15.4	3.9	53.5	7.0	7.9	1

CHAPTER 5
THE EFFECTS OF ATMOSPHERE COMPOSITION

5.1 Introduction

A method called pre-ceramic polymer process to sinter SiC at 1050 ºC was used in this work, since this method does not require high temperature processing or a large amount of sintering additives. The commercialized polymer precursor used to fabricate the SiC pellets is called SMP-10 (allyl-hydrido-poly-carbo-silane). The polymer precursor which contains carbon, silicon and hydrogen, undergoes a polymer to ceramic conversion under heat treatment. In an inert atmosphere, the polymer precursor becomes cross-linked at the curing temperature 180 ºC-400 ºC and produces amorphous silicon carbide which has a 1:1 silicon to carbon atomic ratio at 850 ºC-1200 ºC. [35] This SiC synthesis method to use pre-ceramic polymer precursor (PPP) was systematically studied by Chunghao Shih, a member of Dr Baney's group.

Air was used in the previous work to oxidize SiC. It was found that the corrosion rate in air was low, which may not be practical from an engineering perspective. Multiple oxidizers are evaluated in this work in order to accelerate the process. An unsolved question in the previous work is whether CO_2 is a counter factor for SiC corrosion in the molten K_2CO_3 salt 1050 ºC, since CO_2 can be generated by carbonate decomposition, O_2 dissolution and SiC corrosion in the salt. [83] Moreover, it has been confirmed that O_2 solubility in the molten carbonates can be affected by CO_2 partial pressure below 950 ºC. [84-85] The effect of CO_2 on O_2 solubility at higher temperatures has not been reported. Both questions are addressed in this chapter in order to obtain a better understanding of the SiC corrosion mechanism in the molten K_2CO_3 salt at 1050 ºC. Water vapor has been reported as a more efficient oxidizer for SiC than O_2 above 1000

ºC. However, no systematic investigation has been done on the role of water vapor in the SiC corrosion process. Water vapor is firstly introduced in the SiC/K_2CO_3 corrosion system in order to determine whether water vapor can accelerate the SiC reprocessing process. The SiC reaction rates under different atmospheres such as Ar/O_2, Ar/CO_2, O_2/CO_2, Ar/H_2O, O_2/H_2O and CO_2/H_2O are compared in this chapter to determine the most efficient atmosphere for reprocessing SiC IMFs.

5.2 Results and Discussion

Fabricated SiC pellets used in the corrosion experiment contained β phase and the amorphous phase which originated from the polymer precursor. They had a uniform relative density at 80% and the same dimension (height: 3 mm, diameter: 12.7 mm). Little size shrinkage was found after sintering at 1050 ºC, since the heating temperature is too low to allow grain growth or pore elimination. However, the amorphous SiC network generated by the polymer precursor during the curing stage connected the adjacent SiC particles to form a solid compact [10, 11]. The microstructure of a cross section of a SiC pellet was examined by scanning electron microscopy, as shown in Figure 5-1. SiC particles with two different sizes (16.9 μm and 0.6 μm) were found to be dispersed uniformly in the amorphous SiC matrix.

5.2.1 Air

The calcinated SiC samples were corroded in the molten K_2CO_3 salt with different salt depths from 2 mm to 6 mm in order to confirm whether the corrosion kinetics of the synthesized pellets also follows Fick's diffusion law. After corrosion in air for 4 h, the SiC corrosion rate was linearly reduced by increasing the molten salt depth, as shown in Figure 5-2. This result indicated that Fick's first law could be used to predict the corrosion kinetics of SiC fabricated using different routes. The cross section of a SiC

pellet before and after corrosion in air at 1050 ºC for 4 h were shown in Figure 5-3. The upper surface of SiC became rough after corrosion. The surface indexes of the SiC pellet before and after corrosion were 1.7±0.1 and 5.5 ±1.2, respectively. The existing open pores provided diffusion paths for ions and molecules. Corrosion was more severe at grain boundaries and amorphous phase due to high surface energy and reactivity.

5.2.2 O_2/Ar and CO_2/Ar Atmospheres

In O_2 or CO_2 atmosphere, SiC undergoes an oxidation, as shown below:

$$SiC(s) + 3/2O_2(g) = SiO_2(s) + CO(g) \quad (5\text{-}1)$$

$$SiC(s) + 3CO_2(g) = SiO_2(s) + 4CO(g) \quad (5\text{-}2)$$

The generated silica layer can be dissolved in the molten K_2CO_3 salt at 1050 ºC to form the potassium silicate. The initial molten salt depth was kept constant at 3 mm for the following tests. The experiment on SiC corrosion in the molten K_2CO_3 salt for 4 h under the UHP Ar atmosphere provided a baseline for the kinetic analysis of SiC pellet corrosion. The average weight loss of the SiC pellets was less than 1% in Ar. This result indicated that the amount of CO_2 generated by carbonate decomposition in 4 h was not sufficient to cause severe corrosion of the SiC pellets. Another possible explanation is that due to the low partial pressure of CO_2 in the UHP Ar atmosphere, CO_2 was rapidly removed from the salt by the flowing Ar gas. This result also verified the feasibility of terminating corrosion by replacing the reactive gases by Ar.

The reaction rate of the SiC pellets was found to increase with increasing the molar percent of oxidizers (O_2 and CO_2) diluted by Ar illustrated in Figure 5-4. This result can be predicted by the diffusion law that the flux of the oxidizers approaching the SiC samples is proportional to the concentration of the oxidizers in the salt, which

depends upon their partial pressure in the gas atmosphere. Under a CO_2/Ar atmosphere, the rate followed a linear law at an elevated CO_2 partial pressure. This result again verified that oxidizing gas diffusion is the limiting factor of SiC corrosion in molten K_2CO_3 salt at 1050 ºC. The corrosion rate of SiC pellets under O_2/Ar atmosphere did not appear to follow a linear trend. This result may be attributed to the O_2 dissolution reaction in the salt. The solubility of oxygen in carbonates has been reported to be controlled by a reaction with the melt to generate peroxide (O_2^{2-}) and superoxide (O^{2-}) ions: [78, 84-85]

$$O_2(g) + 2CO_3^{2-}(l) = 2O_2^{2-}(l) + 2CO_2(g) \quad (5\text{-}3)$$

$$O_2(g) + O_2^{2-}(l) = 4O^{2-}(l) \quad (5\text{-}4)$$

Peroxide is the major product in the potassium-rich molten salts. The concentration of O_2^{2-} depends on the partial pressure of O_2 and CO_2, which is mathematically expressed below:

$$[O_2^{2-}] = KP_{O_2}^{0.5} P_{CO_2}^{-1} \quad (5\text{-}5)$$

Assuming that CO_2 gas generated from the O_2 dissolution reaction, once released into the O_2/Ar atmosphere was immediately removed by the flowing gas, formation of O_2^{2-} would be a rapid process which is affected by the partial pressure of O_2 in the atmosphere. It is obvious in equation 5-5 that the O_2^{2-} concentration and the O_2 partial pressure do not have a linear relationship. This non-linear trend indicates that dissolution of O_2 in the salt through the chemical reactions may be significant.

It is shown in Figure 5-4 that O_2 is a more efficient oxidizer than CO_2 at 1050 ºC. Besides the more active oxygen in O_2 compared to CO_2, this might be also because O_2 is in the form of O_2^{2-} in the salt due to O_2 dissolution. SiC can be oxidized by O_2^{2-}:

$2O_2^{2-}(l) + SiC(s) = SiO_3^{2-}(l) + CO(g)$ (5-6)

Both products generated in O_2 and CO_2 atmospheres were amorphous which were shown in Figure 5-5. A trivial amount of unknown crystalline phases was also detected.

5.2.3 O_2/CO_2 Atmosphere

Based on equation 5-5, oxygen solubility in the molten carbonate will increase with increasing partial pressure of O_2 and decreasing partial pressure of CO_2 in the atmosphere. The SiC reaction kinetics in a mixture gas of O_2 and CO_2 was studied in order to determine if the solubility of O_2 in the salt at 1050 ºC affects the SiC reaction rate. The ideal SiC weight loss (labeled as Ideal) curve of the atmosphere of O_2/CO_2 is extrapolated by connecting the two points which represent the weight losses in pure CO_2 and pure O_2, respectively. The experimental SiC weight loss in 4 h as a function of the O_2 molar percent in the O_2/CO_2 atmosphere was compared to the ideal weight loss in Figure 5-6. The actual SiC weight loss (labeled as Experimental) appears to be lower than the theoretical value. Based upon the previous discussion, this result implied that the SiC reaction kinetics is governed by O_2 diffusion in K_2CO_3 at 1050 ºC, which was affected by the O_2 dissolution reaction with the molten carbonate.

5.2.4 H_2O/Ar Atmosphere

Silicon carbide oxidation can be enhanced by water vapor equal to or above 1050 ºC[48]:

$SiC(s) + H_2O(g) = SiO_2(s) + CO(g) + H_2(g)$ (5-8)

Water vapor accelerated SiC corrosion in K_2CO_3 salt, as illustrated in Figure 5-7. Complete SiC corrosion was achieved in 1 h under approximately 80% H_2O/Ar atmosphere, which was at least 4 fold faster than the reaction in 80% O_2/Ar gas.

According to the diffusion law, the weight loss of the SiC samples should have a linear function with the molar percent of water vapor. However, this result was not observed in the experiment. Corrosion was very slow at a lower molar percent of water vapor. The corrosion rate dramatically increased at a higher H_2O molar percent around 60%. At different partial pressure of water vapor, the weight loss was low at beginning as shown in Figure 5-8. The rate increased slowly as the reaction time increasing with a low molar percent of water vapor. On the contrary, the change of the reaction rate with a higher H_2O molar percent was significant as a function of time.

It has been reported that water vapor can dissolve in the molten carbonates to generate potassium bicarbonate ($KHCO_3$), potassium hydroxide (KOH) and carbon dioxide (CO_2) [86-87]:

$$2H_2O(g) + 2K_2CO_3(l) \leftrightarrow 3KOH(l) + KHCO_3(l) + CO_2(g) \quad (5\text{-}9)$$

Potassium bicarbonate is easily decomposed at 1050 ºC [88]:

$$2KHCO_3(l) \leftrightarrow K_2O(l) + H_2O(g) + 2CO_2(g) \quad (5\text{-}10)$$

Potassium oxide can react with water vapor to form potassium hydroxide [66]:

$$K_2O(l) + H_2O(g) \leftrightarrow KOH(l) \quad (5\text{-}11)$$

Unlike O_2, H_2O dissolution in the molten salt cannot generate more active oxidizers. Water molecules may be substantially consumed by the reactions with the salt. Little water could diffuse through the molten salt to contact with the SiC surface. This assumption explained the low corrosion rate with lower H_2O molar percent and at the beginning of corrosion, shown in Figure 5-7 and 5-8. When the salt was saturated by water or the water dissolution reactions reach equilibrium, water could diffuse into the salt as intact molecules which can oxidize SiC rapidly.

In order to prove this hypothesis, the K_2CO_3 salt without SiC was heated in the tube furnace at 1050 ºC for 1 h under air and 80% H_2O/Ar, with the same total flow rate. The residual salt was cooled down to room temperature in UHP Ar flow, followed by XRD examination. The XRD spectra of both salt residues were shown in Figure 5-9 and 5-10. The composition of the salt after heating in air for 1 h was barely changed, which was still K_2CO_3 as shown in Figure 5-9. A small amount of KOH was also detected, possibly due to the hydrolysis of K_2O generated from K_2CO_3 decomposition. On the contrary, the salt after heating in 80% H_2O/Ar for 1 h primarily consisted of amorphous phase and KOH, as shown in Figure 5-10. A trivial amount of K_2CO_3 was detected as well since KOH readily absorb CO_2 in air forming K_2CO_3. The amorphous phase was comprised of K, O and Al, which indicated the alumina was dissolved in the formed KOH due to water vapor dissolution in the salt. This observation confirmed that water vapor dissolved in the K_2CO_3 molten salt through reactions in which large amount of caustic KOH was generated due to water consumption.

5.2.5 H_2O/O_2 and H_2O/CO_2 Atmospheres

Weight loss percent of the SiC samples after corrosion for 0.5 h in H_2O/O_2 was almost constant as increasing the H_2O molar percent up to 80%, as shown in Figure 5-11. This result indicates that the effect of increasing water vapor concentration on the SiC reaction rate was offset by the effect of decreasing oxygen concentration. In a limited reaction time, the amount of water vapor supplied into the system was not sufficient to saturate the molten salt, causing rapid SiC oxidation. Therefore, the acceleration effect attributed to water vapor was not significant. When the reaction was extended to 1 h, the weight loss value was doubled, but still remained constant until the H_2O concentration was higher than 60%. This phenomenon can also be explained by

the earlier presented theory. Above 60%, the SiC corrosion rate was significantly increased with increasing H_2O molar percent. This observation was consistent with the result obtained in H_2O/Ar gas. Surprisingly, the corrosion rate appeared to be higher under the H_2O/CO_2 atmosphere than in the H_2O/O_2 atmosphere. Carbon dioxide is a product of the water dissolution reaction with the salt as described in equation 5-9 and 5-10. Presence of CO_2 in the H_2O/CO_2 atmosphere may hinder the water/salt reaction, which allows water vapor to diffuse into the salt as intact molecules. Such enhancement effect contributed by CO_2 was eliminated with decreasing the CO_2 concentration. Based on the limited data, the curve of the SiC weight loss in H_2O/CO_2 appeared to approach to the curve of H_2O/O_2 as an increase in the H_2O concentration. More data are required to accurately simulate such trend.

5.2.6 H_2O/CO_2 Atmosphere with Various Total Flow Rates

Studies on various H_2O/CO_2 total flow rate were performed in order to optimize the conditions for reprocessing the SiC IMFs. Figure 5-12 shows the weight loss percent of the SiC specimens in 1 h under H_2O/CO_2 atmosphere with multiple H_2O molar percent as a function of total flow rates. With a lower total flow rate, the SiC reaction rate was considerably lower. This result may be because the supply of water vapor in 1 h was not sufficient to saturate the molten salt even with high water vapor concentration. Flow rate increase allowed large amount of water vapor to continuously diffuse into the molten salt, which enhanced the SiC oxidation and dissolution in the molten salt. Moreover, a decrease of the molten salt depth due to K_2O volatilization and salt decomposing into K_2O and CO_2 could also contribute to the increase in the SiC weight loss. It has been accepted that the volatilization rate at high temperature depends upon the mass transferring diffusion which can be enhanced by the convection in the gas

phase. [89] CO_2 gas generated by salt decomposition was rapidly removed in the gas flow, which further accelerates the salt loss. The amount of salt needed to be saturated by water vapor was consequently reduced, since the molten salt depth decreasing was enhanced in a rapid gas flow. As a conclusion, sufficient water supply and continuous molten salt depth decrease resulted into the high SiC weight loss in 76% H_2O/CO_2 and 69% H_2O/CO_2 with increasing the total flow rate.

However, the SiC pellet weight loss in 76% H_2O/CO_2 and 69% H_2O/CO_2 decreased at a higher total flow rate after reaching to a maximum value. This phenomenon may be because the SiC samples were exposed in the gas phase due to rapid salt loss, which was observed in experiments. SiC corrosion was consequently terminated. The SiC corrosion in 76% H_2O/CO_2 ceased at a lower flow rate compared to 69% H_2O/CO_2 since the salt loss was more significant with a low CO_2 partial pressure.

5.3 Conclusions

The molten salt corrosion method for reprocessing the SiC IMFs was initiated and systematically developed in the early and current work. Various gases which may be more efficient than air were studied. The order of the corrosion rates under the CO_2, O_2 and H_2O atmospheres is:

Carbon dioxide < Oxygen < Water vapor

The SiC corrosion rate depends upon the molar percentage of the oxidizers (CO_2, O_2 and H_2O) in the atmosphere. Dissolution reactions of O_2 with the molten K_2CO_3 salt may affect SiC corrosion. The SiC reaction kinetics in CO_2/H_2O, O_2/H_2O and CO_2/O_2 were studied as well. Water vapor with CO_2 seems to be the most efficient among those gas mixtures. An increase in the total flow rate accelerated the SiC corrosion. However, excessive flow rate caused SiC reaction termination.

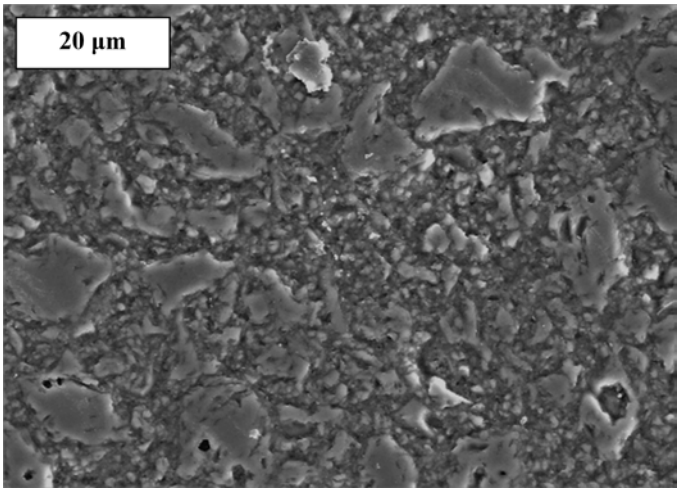

Figure 5-1. Microstructure of the cross-section of a synthesized SiC pellet

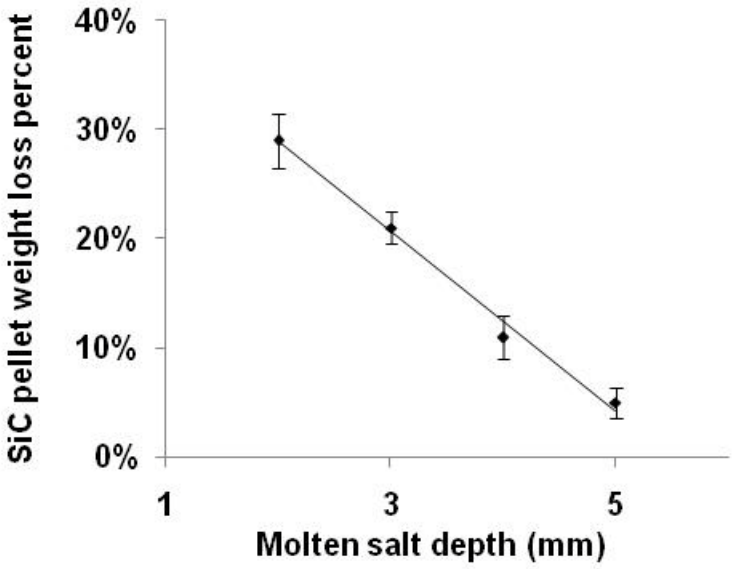

Figure 5-2. Weight loss of calcinated SiC pellets corroded in the molten K_2CO_3 salt at 1050 ºC for 4 h in air as a function of salt depth

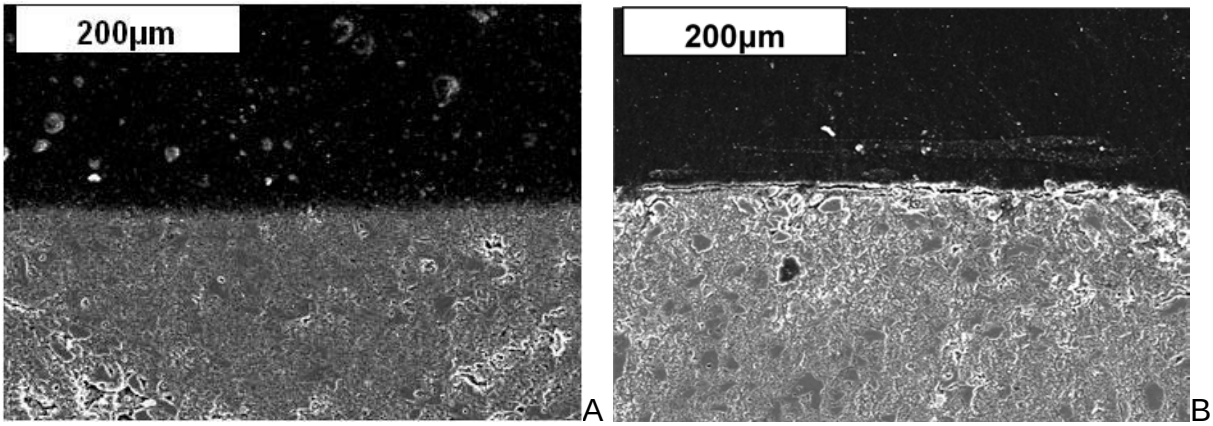

A B

Figure 5-3. Microstructure of cross section of a SiC pellets before and after corrosion in air at 1050 ºC for 4 h; A) before corrosion B) the top area after corrosion

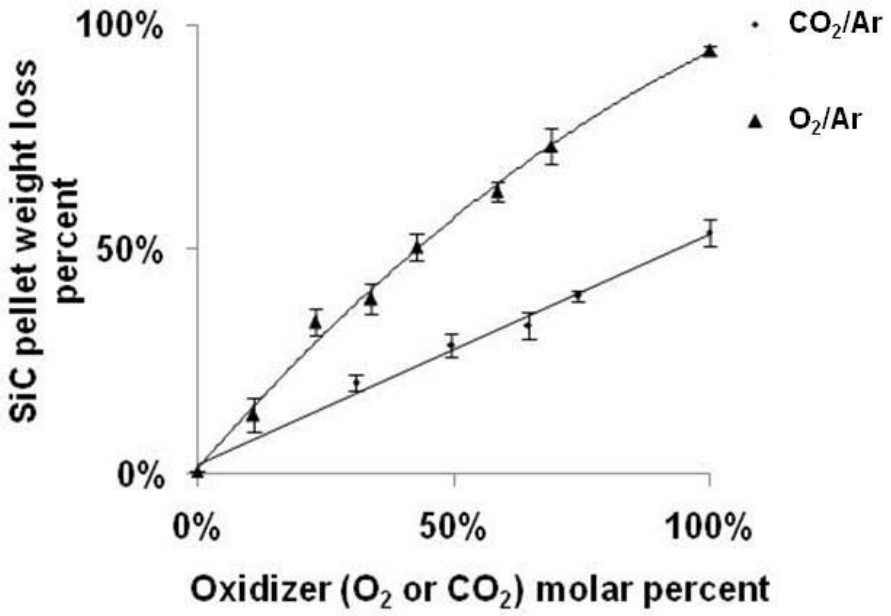

Figure 5-4. SiC pellet weight loss after corrosion in K_2CO_3 at 1050 ºC in gas mixtures of O_2/Ar and CO_2/Ar for 4 h as a function of O_2 and CO_2 molar percent, respectively

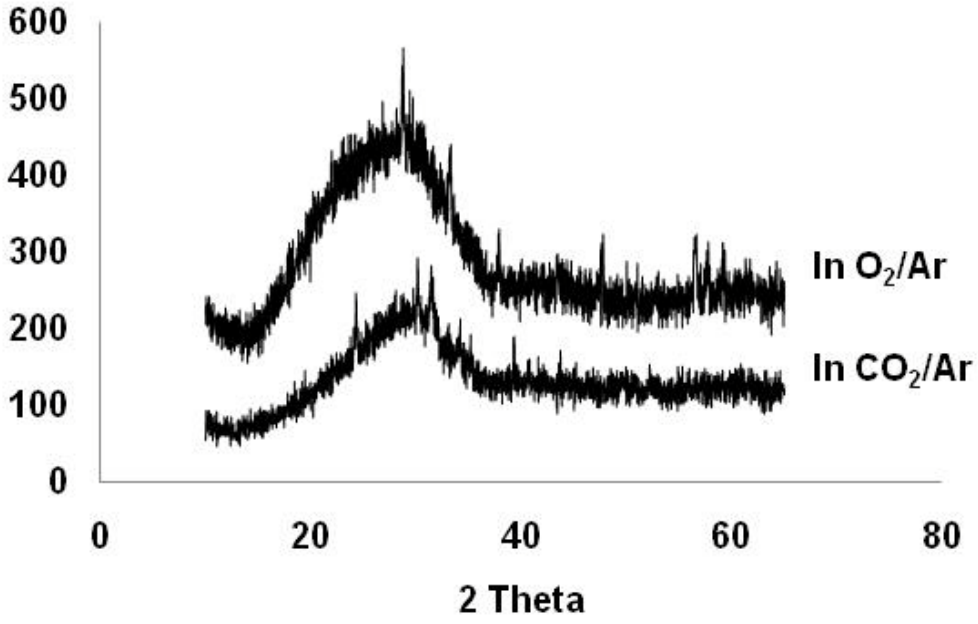

Figure 5-5. XRD spectra of products of SiC/salt reaction at 1050 ºC in O_2/Ar and CO_2/Ar atmospheres

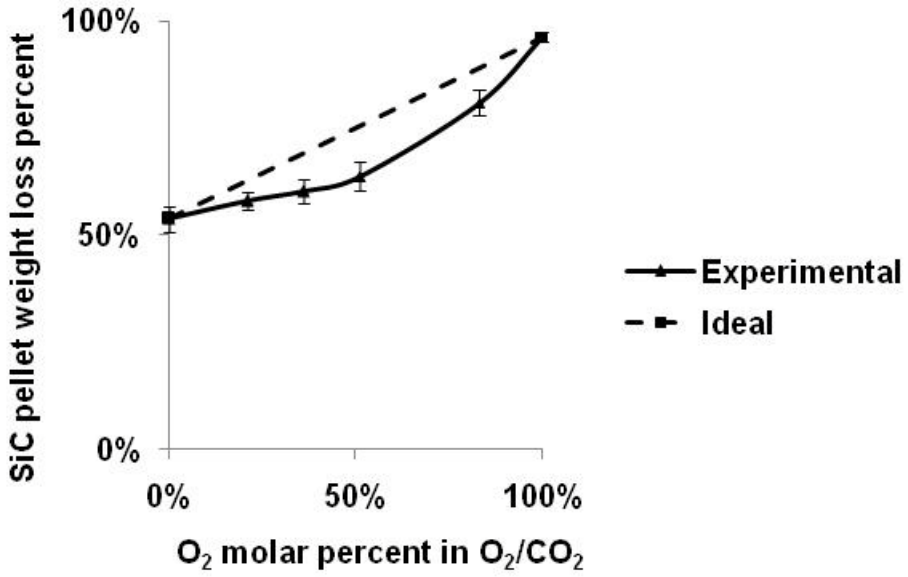

Figure 5-6. Weight loss percent of SiC pellets after corrosion in K_2CO_3 at 1050 ºC in a gas mixture CO_2/O_2 for 4 h as a function of O_2 molar percent

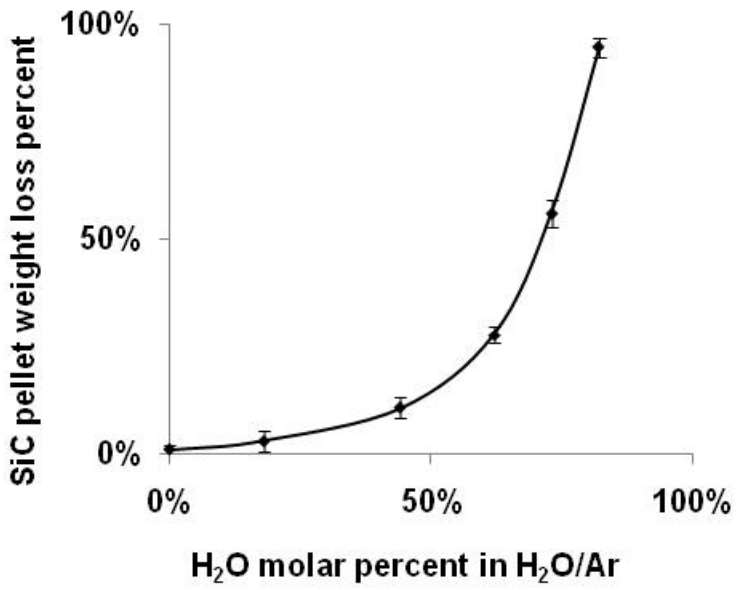

Figure 5-7. Weight loss percent of SiC samples after corrosion in K_2CO_3 at 1050 ºC in a gas mixture H_2O/Ar for 1 h as a function of H_2O molar percent

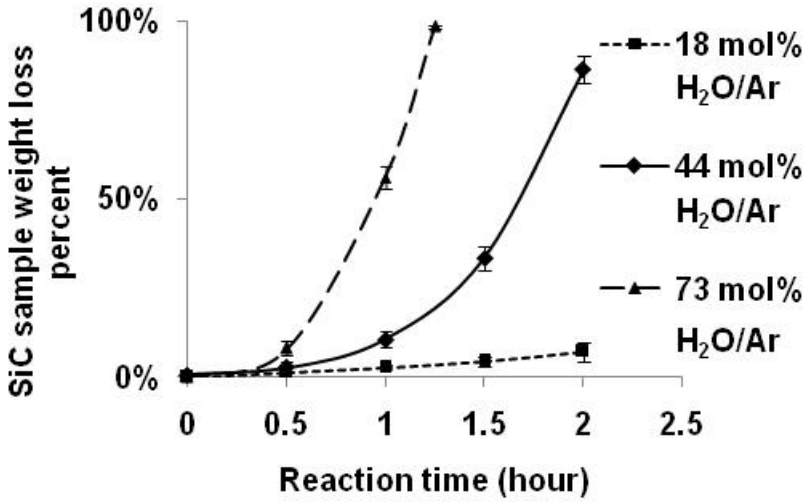

Figure 5-8. Weight loss percent of SiC samples after corrosion in K_2CO_3 at 1050 ºC in H_2O/Ar with different water molar percent as a function of the reaction time

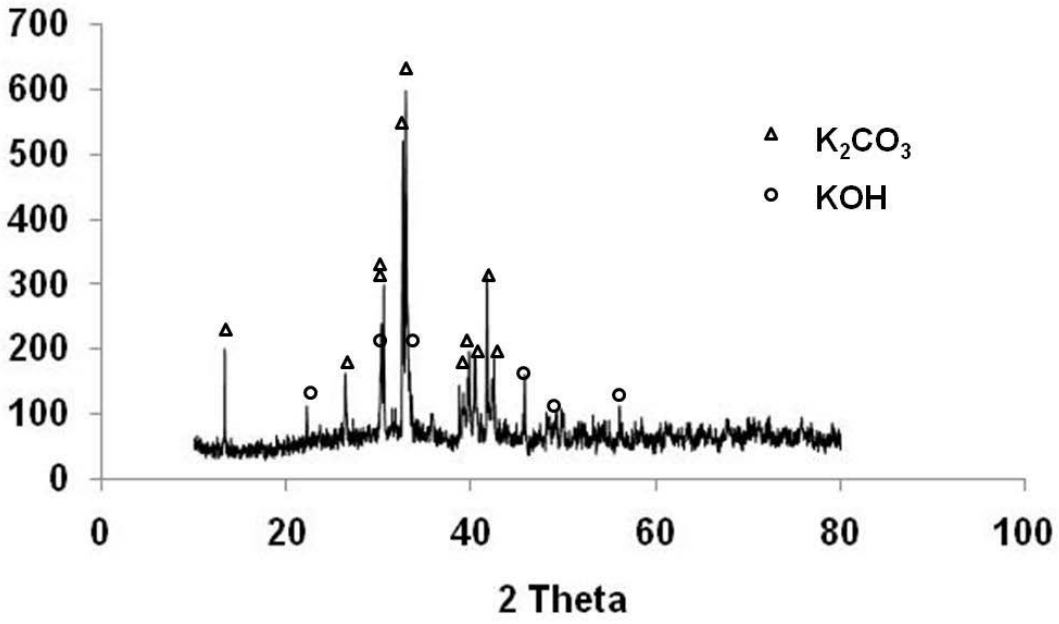

Figure 5-9. XRD spectra of K_2CO_3 salt exposing in air for 1 h and the products are K_2CO_3 and KOH

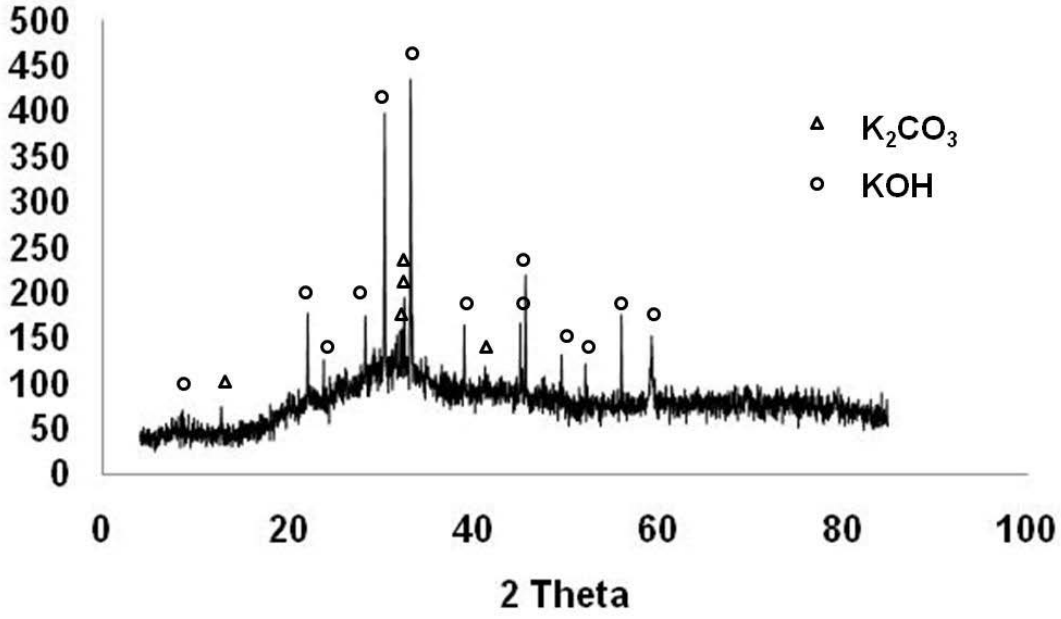

Figure 5-10. XRD spectra of K_2CO_3 salt exposing in 80% H_2O/Ar for 1 h and the products are KOH, an amorphous phase and a small amount of K_2CO_3

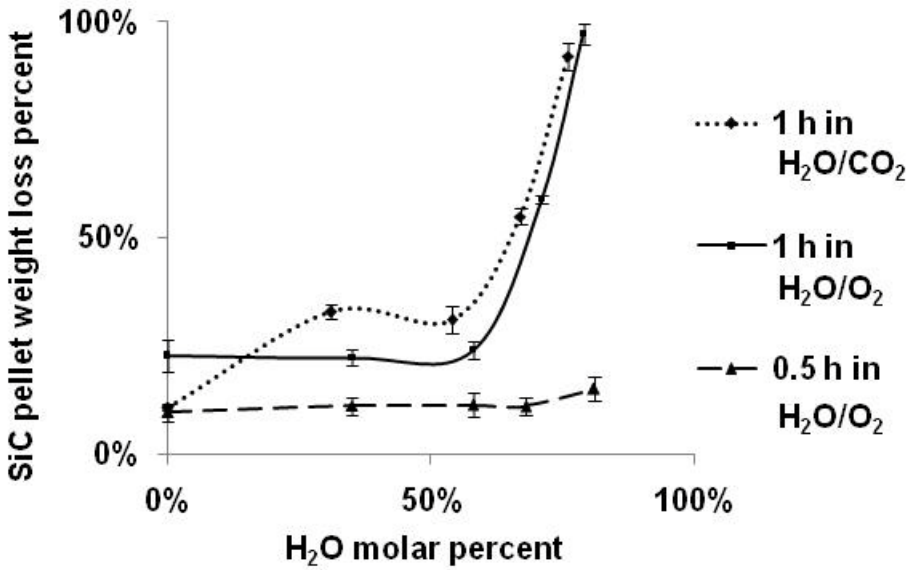

Figure 5-11. Weight loss percent of SiC samples after corrosion in K_2CO_3 at 1050 ºC in H_2O/CO_2 and H_2O/O_2 as a function of H_2O molar percent

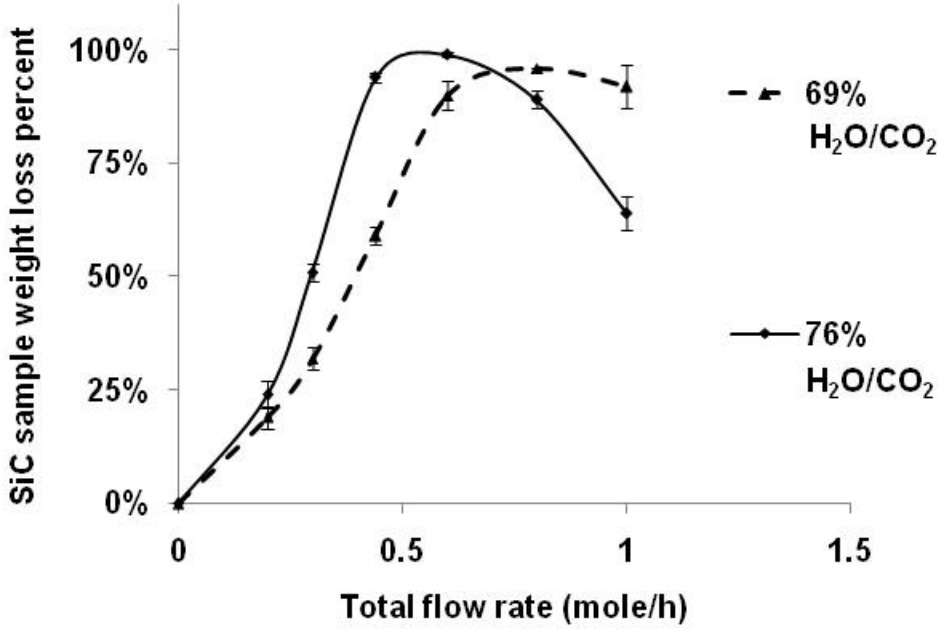

Figure 5-12. Weight loss percent of SiC samples in K_2CO_3 at 1050 ºC in 1 h under H_2O/CO_2 with different H_2O vapor concentrations as a function of the total flow rate

CHAPTER 6
REACTION BEHAVIOR OF CERIA IN THE MOLTEN SALTS

6.1 Introduction

Non-radioactive metal oxides are usually utilized in the research of radioactive waste treatment in order to minimize the environmental impact and hazardous level. For each radio-nuclide, the primary criterion of selecting the corresponding non-radioactive surrogate is based on their common oxidation state. [90] Ceria (CeO_2) has been widely used as a surrogate for plutonium oxide (PuO_2). [91-94] Both CeO_2 and PuO_2 have the fluorite-type crystal structure. [94] They also have similar thermal dynamic properties such as Gibbs free energy of formation (ΔG formation), which indicates a fundamental basis for selecting CeO_2 as a substitute of PuO_2. [93] The following reaction is used to calculate ΔG formation:

$$\frac{2x}{y}M + O_2 = \frac{2}{y}M_xO_y \qquad (6\text{-}1)$$

Where x and y are arbitrary values representing for the stoichiometry of the metal oxides and M are Ce and Pu, It has been reported that both oxides show approximately identical weight and dimension decreasing when sintering from 1000 ºC to 1700 ºC under Ar-6% H_2 atmosphere, which suggests a similarity of sintering behaviors of CeO_2 and PuO_2. [91, 93] The weight loss in the reducing atmosphere is based on the following reactions:

$$2MO_2(s) + H_2(g) = M_2O_3(s) + H_2O(g) \qquad (6\text{-}2)$$

$$2M_2O_3(s) = 4M(s) + 3O_2\ (g) \qquad (6\text{-}3)$$

Therefore, CeO_2 was used in this work as a surrogate for PuO_2 to test the feasibility of the molten salt corrosion method for reprocessing SiC IMFs.

6.2 Experimental Procedures

6.2.1 Reaction Behavior of CeO_2 in Molten Carbonates

CeO_2 powder and pellets were purchased from Alfa Aesar. Experiments on ceria fine powder (5-9 μm) and ceria pellets (theoretical density: 88%; purity: 99.9%; metal basis) corroded by alkali salts (Na_2CO_3 and K_2CO_3) at a 10:1 molar ratio to CeO_2 were performed at 1050 ºC up to 15 h under various atmospheres (air, Ar/O_2, Ar/CO_2, Ar/H_2O, and CO_2/H_2O). Experimental parameters are demonstrated in Figure 6-1. The specific experiment design was summarized in Table 6-1.

Three parallel tests were performed for each reactant combination to determine the mean value. The initial weight of the ceria powder and the ceria pellet were approximately 0.5 g and 3 g for each experiment. The weight difference was measured between the original ceria and the residue ceria after washing away the alkali salts. The ceria pellets were dried in the vacuum oven at 6800 Pa for 12 h at 80 ºC to remove the water absorbed in open pores. The average ceria weight change percent was calculated at the end. Blank experiments on CeO_2 powder were also performed. The CeO_2 weight change, due to ball milling, transferring the powder from one container to another and washing, was measured to determine the operation error of the weight change measurement.

6.2.2 Fabrication of SiC/CeO_2 Pellets

SiC powders with 16.9 μm (coarse) and 0.6 μm (fine) nominal particle size were mixed at a 3:2 weight ratio with 10 wt% of SMP-10 and 5 wt% of CeO_2 powder (from Alfa Aesar) with a size of 70-100 nm in a ball miller for 1 h. The amount of CeO_2 powder was fixed at 5 wt% in order to be consistent to the PuO_2 amount in the MOX fuels. The slurry was pressed into pellets (height: 3 mm, diameter: 13 mm) at 600 MPa in a cold

uniaxial pressing equipment. The green compacts were then calcinated in an alumina tube furnace up to 1050 ºC with a constant UHP Ar flow. Air in the furnace was removed by flowing UHP Ar for 2 h before heat treatment. The same sintering temperature profile applied in the SiC fabrication described in chapter 3 was followed. The SiC/CeO_2 fabrication method was systematically studied by Chunghao Shih, a member of Dr Baney's group. [99] The bulk density can be determined from the volume and weight.

6.2.3 Reprocessing SiC/CeO_2 Pellets

Based on the studies discussed in early chapters, the optimized processing conditions for reprocessing the SiC based IMFs should be:

1. To use the K_2CO_3 salt with a molar ratio to SiC higher than 1 e.g., 2,
2. To use the K_2CO_3 salt with a shorter salt depth e.g., 3 mm, in a condition that specimens should be thoroughly immersed in the molten salt throughout the reaction,
3. To use the H_2O as the reaction atmosphere,
4. To use a moderate gas flow e.g., 0.6 mol/h,
5. To use 1050 ºC as the reaction temperature.

The above conditions were applied in order to separate CeO_2 powder from the SiC matrix. After reaction, the formed precipitate was dissolved in 50% KOH solution in 1 min under stirring. The CeO_2 powder was separated from the washing solution by centrifuging at 10000 rpm for 5 min, followed by drying in a vacuum oven at 120 ºC. The average weight loss was obtained.

6.3 Results and Discussion

6.3.1 Ceria in Molten Carbonates

The experimental results are summarized in Table 6-2 for the ceria powder (5-9 µm). The pellets did not have a significant weight change. The XRD spectra in Figure 6-

2 did not show new phases generated in molten salt corrosion tests, which confirms that ceria does not react with the molten salt at 1050 ºC. The reason for using ceria powder is that fine powders are expected to have much higher reactivity than bulk material due to the higher specific surface area and thus the higher surface free energy. The weight loss of ceria powder after corrosion in the molten salt was negligible and approximately equaled to the ceria weight loss caused by handling error. The ceria pellets in the molten salts also showed negligible weight changes. The slight weight increase (0.0001~0.0006 g) of ceria pellets may be because water penetrating into the ceria open pores in the washing step would be difficult to be removed away completely from the ceria body, considering the low theoretical density (88%) of ceria pellets. This hypothesis was verified by experimental results that higher vacuum (3400 Pa) applied on ceria pellets for 24 h resulted in complete weight recovery of ceria pellets. Due to plutonium oxide's similar chemical properties to ceria, it is expected that bulk plutonium oxide will not dissolve in this molten salt process. This result indicates the feasibility of the molten salt corrosion method in which SiC is corroded in K_2CO_3 molten salt to form the water soluble silicates but ceria is unchanged at 1050 ºC.

6.3.2 Characterization of SiC/CeO_2 Pellet

6.3.2.1 Density

Relative density (RD) of a SiC/CeO_2 pellet can be calculated by using the following equation:

$$RD = \frac{\rho_{mea}}{\rho_c} \times 100\% \tag{6-4}$$

$$\rho_{mea} = \frac{W_s}{V_s} = \frac{4W_s}{\pi d^2 h} \tag{6-5}$$

$$\rho_c = 95\%\rho_{ref,SiC} + 5\%\rho_{ref,CeO_2} \quad (6\text{-}6)$$

Where RD is relative density, ρ_{mea} is the density of the SiC/CeO_2 pellet being measured, ρ_{ref} is the calculated density of a fully dense SiC/CeO_2 pellet, ρref, SiC is the density of a fully dense SiC which is 3.21 g/cm^3, ρ_{ref}, CeO_2 is the density of a fully dense CeO_2 with a fluorite phase which is 7.22 g/cm^3, W_S is the weight of the SiC/CeO_2 specimen and d and h are the diameter and height of the SiC/CeO_2 specimen, respectively, which can be determined by using a caliper. All SiC/CeO_2 specimens had a relative density at 81%.

6.3.2.2 Microstructure

As shown in Figure 6-3, the microstructure of a SiC/CeO_2 pellet was examined by using back-scattering SEM due to the atomic weight difference of SiC and CeO_2. The white dots and dark regions in images are CeO_2 powder and SiC grains respectively. The gray interphase is amorphous SiC originated from the pre-ceramic polymer precursor. CeO_2 powder was homogenously distributed in the SiC matrix. Several big agglomerations of CeO_2 particles were also found in the images.

6.3.3 Reprocessing SiC/CeO_2 Pellets

The white precipitate was also found when dissolving the residues in boiling water. The XRD and EDS spectra confirmed that this product was amorphous which consisted of K, Al, Si and O. Due to the limited reaction time, no crystalline phase was generated in the salt bath, as shown in Figure 6-4.

It has been reported that CeO_2 can react with SiO_2 in a reducing or inert atmosphere (H_2/N_2 or Ar) above 1000 ºC forming cerium silicates. [96-98] Such reaction does not occur in an oxidizing atmosphere (air) below 1400 ºC. A comparatively low

reaction temperature and an oxidizing atmosphere used in the reprocessing experiment prevented the SiO_2/CeO_2 reaction even if a great amount of SiO_2 was generated as an intermediate product in this process, since no cerium silicate phase was detected in the residue by using XRD. No cerium was detected in the washing solution using ICP. The weight difference between the recovered ceria powder and the initial ceria mixed with the SiC powder was -1.0% $\pm$ 0.3%. This trivial amount of weight loss is handling error which was verified in the blank experiment in which the weight loss of ceria powder due to ball milling, slurry collection from the milling jar, washing and transferring was obtained.

6.4 Conclusions

Ceria/salt reaction did not occur under different oxidizing atmospheres at 1050 ºC, No weight change or phase change of ceria specimens was found. Ceria powder was successfully separated from the SiC matrix under the proposed reprocessing conditions. These results confirmed the feasibility of the molten salt reaction/dissolution method for reprocessing SiC IMFs.

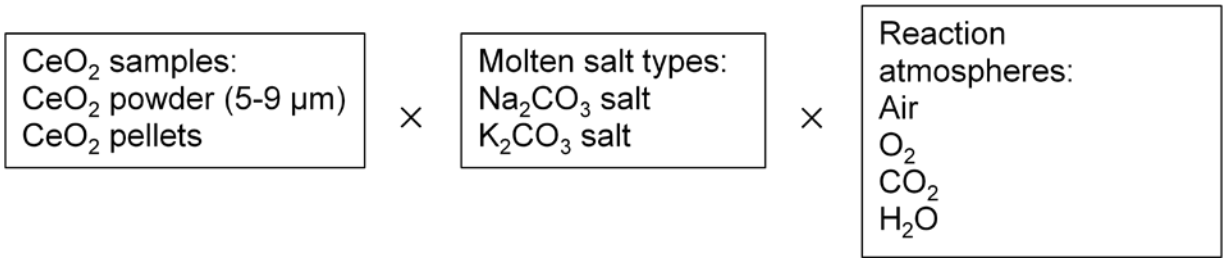

Figure 6-1. Scheme of experiments of CeO_2 powder and pellets in two types of molten salts and multiple reaction gases

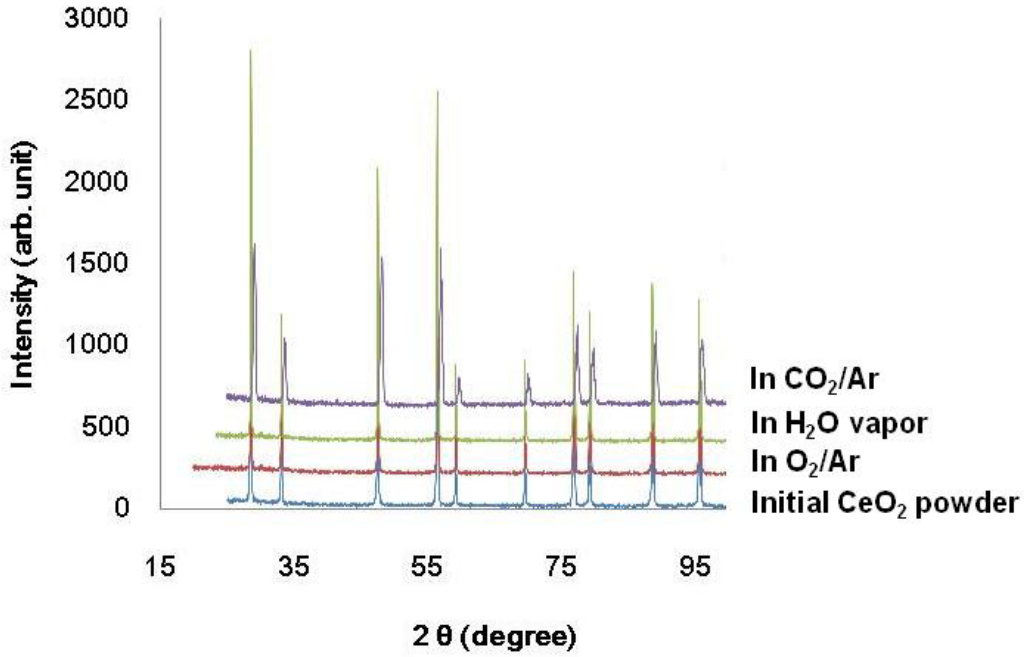

Figure 6-2. XRD spectra of the CeO_2 powder (5-9 μm) after corrosion in the K_2CO_3 salt at 1050 ºC up to 10 h

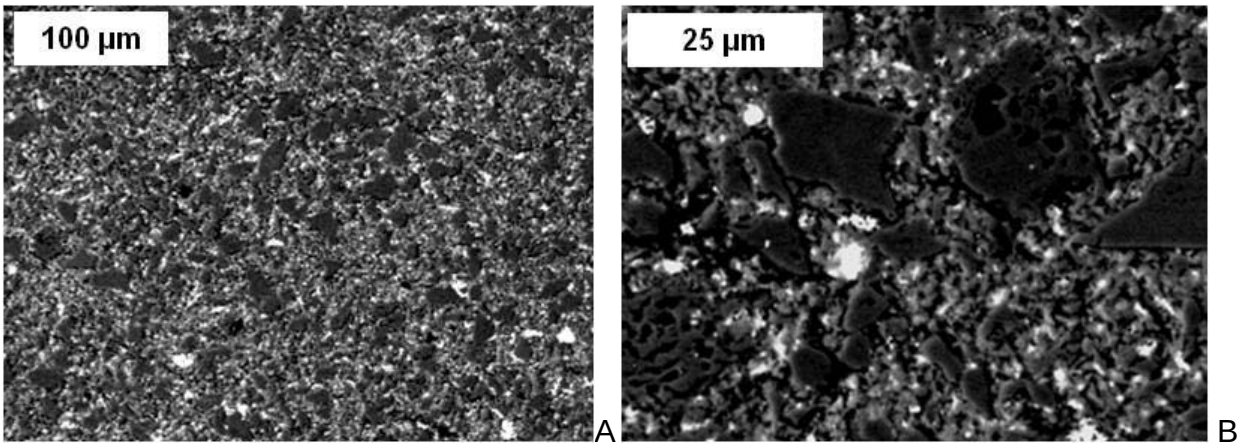

A B

Figure 6-3. Back-scattering images of the cross section of a synthesized CeO_2/SiC pellet at A) lower magnification B) higher magnification

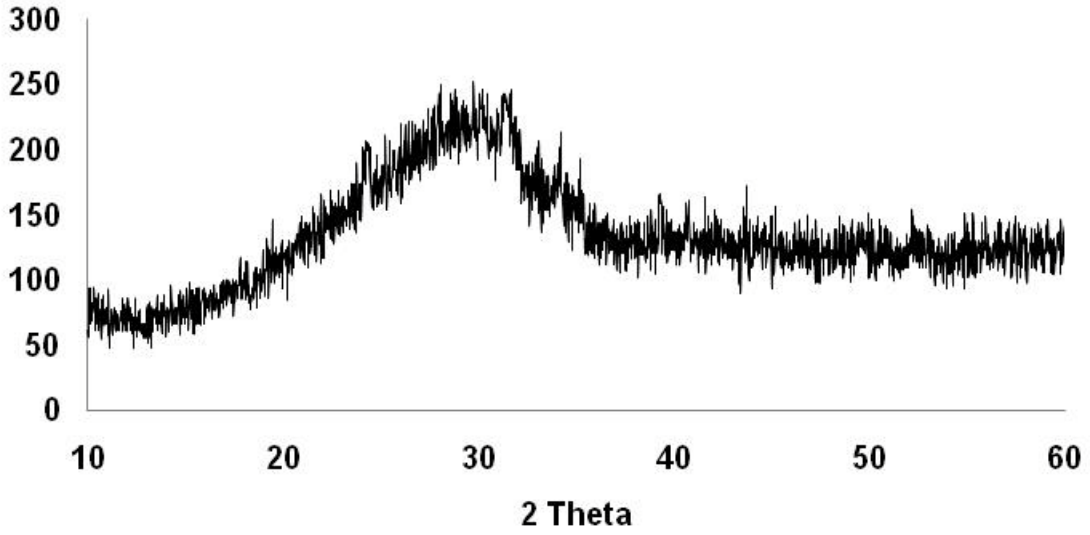

Figure 6-4. XRD spectrum of the product of SiC/CeO_2 reaction in the molten salt under water vapor at 1050 ºC

Table 6-1. Experiment of CeO_2 samples in the molten salts at 1050 ºC

Experiment ID	CeO_2 samples	Molten salts	Atmospheres
00 (Blank)	Powder	N/A	N/A
01	Powder	Na	Air
02	Pellet	Na	Air
03	Powder	K	Air
04	Pellet	K	Air
05	Powder	K	O_2
06	Powder	K	CO_2
07	Powder	K	H_2O
08	Powder	K	80% H_2O/CO_2
09	Pellet	K	O_2
10	Pellet	K	CO_2
11	Pellet	K	H_2O
12	Pellet	K	80% H_2O/CO_2

Table 6-2. Weight change percent of bulk and powder ceria after corrosion in two molten carbonates under multiple atmospheres ("-" represents weight loss and "+" represents weight increase)

Experiments	Ceria weight change percent	Standard deviation
00	-0.60%	0.43%
01	-0.74%	0.14%
02	0.01%	0.01%
03	-0.56%	0.47%
04	0.02%	0.01%
05	-0.86%	0.25%
06	-0.69%	0.42%
07	-0.69%	0.38%
08	-0.82%	0.16%
09	0.03%	0.01%
10	0.02%	0.00%
11	0.02%	0.00%
12	0.01%	0.00%

CHAPTER 7
SUMMARY AND FUTURE WORK

7.1 Summary

The search for a material to function as the matrix in IMFs to reduce inventories of plutonium and to carry out the transmutation of the long half-life actinides has been a goal for several years. Silicon carbide (SiC) has become one of the prime IMF candidate materials, since both silicon and carbon have a small thermal neutron absorption cross section. Silicon carbide is also well known for its chemical inertness, good thermal conductivity and mechanical properties. Not all of the actinides and plutonium will be consumed during an in-core cycle. Therefore, it is necessary to separate the non-transmuted or non-fissioned fuels from the inert matrix for recycling. Reprocessing and separating transuranic species and unburned fuels from a silicon carbide matrix have been a challenge to date because of the excellent chemical inertness of bulk SiC.

Various methods have been considered to separate CeO_2, a surrogate for plutonium oxide, from the SiC matrix. Since SiC does not dissolve in any acid due to its chemical inertness, the traditional reprocessing approach cannot be transferred to the SiC IMFs. SiC can be volatilized in forms of $SiCl_4$, SiO and $Si(OH)_4$ through the reaction with chlorine gas, oxygen and water vapor. However, the SiC volatilization rate is very low even at high temperature. The molten salt corrosion method was selected due to its compatibility with the current nuclear plant and high reaction rate with SiC. The desired salt should have the following properties: low melting point, high boiling point, generating the water soluble silicates after reaction with SiC, no corrosive gas product, no reaction with CeO_2 and rapid reaction with SiC. Sodium and potassium carbonates

were selected in this work. β-SiC was used in this research since its isotropic crystal structure is generally desired for application in the nuclear industry.

The result that SiC fine powder (1 μm) was completely reacted with the Na_2CO_3 sat in 0.5 h at 900 ºC forming water-soluble Na_2SiO_3 indicated the feasibility of the molten salt reaction/dissolution strategy. Homogeneously mixing the SiC and the salt is critical to achieve a high reaction rate. The reaction terminated when the starting materials were not uniformly mixed, which is due to formation of SiC clusters.

Further study was conducted to dissolve the monolithic SiC pellets based on the promising results obtained in the powder work. Little weight loss of the SiC pellets was found under the same experiment conditions as the SiC powder studies, possibly due to the formed solid silicates retarding the ion transportation. This silicate layer can be removed in the molten salts above the melting temperature of silicates. Reprocessing temperature for the bulk SiC in the molten K_2CO_3 salt was increased to 1050 ºC which is above the melting temperature of the potassium silicate layer formed on the SiC surface. A higher processing temperature is required if using the Na_2CO_3 salt according to the Na_2O-SiO_2 phase diagram.

To obtain the silicates with high solubility in water, the molar ratio of salt to SiC should be no less than 1. It was found that when the molten salt depth or gas diffusion distance, which is a distance between the salt/air interface to the upper surface of SiC pellets, was maintained constant, the salt amount had no effect on the SiC reaction rate in both Na_2CO_3 and K_2CO_3 salts. Excess salt is unnecessary to achieve a high reaction rate. Moreover, an increasing SiC reaction rate was observed with a decreasing depth of the molten salt K_2CO_3 and Na_2CO_3 salt at 1050 ºC in air. This result can be explained

by Fick's diffusion law that the oxygen flux depends upon the diffusion gradient and its diffusivity in the salt. The SiC pellets dissolved more rapidly in the molten K_2CO_3 salt than in Na_2CO_3 at 1050 ºC which verified the hypothesis that potassium silicate melting enhanced SiC/salt reaction. Moreover, Na_2O and K_2O generated from carbonate decomposition have very high vapor pressure at 1050 ºC. The salt depth was continuously reduced during reaction due to salt volatilization. While moderate amount of salt is preferred to obtain a short salt depth, SiC samples should be thoroughly immersed in the molten salt during the entire process to progress the reaction.

The SiC samples were synthesized by calcinating a green compact which consisted of a pre-ceramic polymer precursor and SiC fine powder with two different sizes. SiC particles were uniformly dispersed in a SiC amorphous phase originated from the precursor. All SiC samples which had identical dimension and weight were polished by using diamond paste in order to minimize the effect of the surface area difference on the reaction kinetics.

Average weight loss of the SiC pellets was less than 1% in Ar, which built a baseline for the SiC/salt reaction. Reaction rate of the SiC pellets was found to increase with increasing molar percent of the oxidizers, O_2 or CO_2. In a CO_2/Ar atmosphere, reaction rate followed a linear law under an elevated CO_2 partial pressure. The linear law was not applied to the O_2/Ar atmosphere. The reaction rate in O_2/CO_2 cannot be simply extrapolated by using the rates in the pure O_2 and pure CO_2 gases. The actual rate in O_2/CO_2 was considerably lower. The results indicated that CO_2 affected the solubility of O_2 at 1050 ºC which consequently, affected the SiC reaction rate.

Water vapor was first applied into the SiC/carbonates system to accelerate the process. As expected, the reaction rate in water vapor was enhanced about 4 folds compared to the O_2/Ar atmosphere. The SiC pellets totally reacted with the salt in 1 h under the 80% H_2O/Ar atmosphere. Complete reaction at least needs 4 h in the pure O_2 atmosphere. Other than following a linear relationship with the molar percent of water vapor, the reaction rate was very low with a low H_2O concentration but dramatically increased with an elevated H_2O concentration. The rate in water vapor was also a function of time, which was increased as increasing the time. These phenomena may be due to the water vapor/carbonate reactions at 1050 ºC. A similar trend of the reaction rate in both O_2/H_2O and CO_2/H_2O atmospheres was observed as increasing the molar percent of water vapor. However, the SiC pellets appeared to be dissolved more rapidly in CO_2/H_2O than in O_2/H_2O. This result can also be explained by the H_2O/K_2CO_3 reaction since CO_2 is one of the reaction products. Presence of CO_2 in the atmosphere may hinder the H_2O/salt reaction allowing H_2O to diffuse in the salt as intact molecules. The gas total flow rate is another important factor which affects the SiC reaction kinetics. An increase in the SiC reaction rate was found as increasing the total flow rate of CO_2/H_2O, which was more rapidly in the atmosphere with higher water vapor molar content. This phenomenon may be because of the salt loss enhanced by the salt/water reaction and salt volatilization in a convective atmosphere. As a consequence, the molten salt depth and the amount of salt required to be saturated for severe SiC corrosion was decreased. On the other hand, sufficient water vapor was supplied into the salt as increasing the flow rate. Excess salt loss may result into retardation of the SiC reaction since the SiC samples were not immersed in the salt as observed in

experiment. In conclusion, potassium carbonate salt with short salt distance (diffusion distance), sufficient water vapor and moderate gas flow rate are recommended to achieve an efficient reaction rate.

The reaction behavior of ceria fine powder and pellets in both Na_2CO_3 and K_2CO_3 salts under the atmospheres of air, O_2/Ar, CO_2/Ar, H_2O/Ar and CO_2/H_2O at 1050 ºC were investigated in order to assure that ceria can be maintained intact in those proposed reprocessing environments. Weight change of the ceria samples after reaction was trivial. The XRD and ICP results verified that no new ceria phase was generated either in the recycled ceria or in the washing solution. Ceria was successfully separated from the SiC matrix by applying the proposed strategy in the optimal conditions. These results confirmed the feasibility of this molten salt reaction/dissolution method for reprocessing SiC IMFs.

7.2 Future work

7.2.1 Temperature

It has been confirmed in this study that the SiC reaction in the molten salts at 1050 ºC is primarily governed by oxidizing gas diffusion. The temperature effect is necessary to investigate since diffusion is sensitive to temperature change. A linear trend of the SiC weight loss has been observed after exposure in air for extensive time. The SiC weight loss as a function of time from 900 ºC to 1200 ºC will be studied in order to examine if the SiC weight loss increases linearly as time increasing at different temperature. The Arrhenius plot of the reaction rate constant versus temperature will be obtained. The activation energy of the SiC/K_2CO_3 reaction under different atmospheres will be calculated to model the kinetics.

7.2.2 Total Flow Rate of Pure Water Vapor

Total flow rate of H_2O/CO_2 has been verified in this work to be an important factor which affects SiC IMFs reprocessing. Moreover, complete dissolution of the SiC pellets were also achieved in pure water vapor flow without CO_2 in 1 h. It is important to investigate the SiC/salt reaction kinetics with various flow rate of pure water vapor, since supplying water vapor is simpler compared to providing a mixture of H_2O and CO_2.

7.2.3 Silicon Carbide Density

Pre-ceramic polymer precursor was used to fabricate the SiC specimens which had the equal weight, dimension and density. The SiC samples used in this work had a low relative density at 80%. The SiC pellets with higher density are desired in the nuclear industry since the dense pellets have high thermal conductivity, which reduces the centerline temperature of the nuclear fuel as a consequence. Based on Chunghao's work, density of the SiC pellets can be increased by infiltrating more polymer precursor into the open pores, followed by another pyrolysis process. The relative density in a range of 80% to 90% can be achieved depending on the number of cycles of polymer infiltration and calcinations. The reaction rate of SiC specimens with different density will be compared in order to examine the effect of bulk density on the reaction kinetics.

7.2.4 Other Molten Salts

Sodium carbonate and potassium carbonate were used in this research to dissolve SiC because their high reaction rate with SiC, low melting temperature, high boiling temperature and ease of handling. Sodium sulfate has been reported to corrode SiC rapidly as well. This salt was not selected at beginning due to the hazardous gas products such as SO_2 and SO_3. Based on concern of efficiency, this salt is worth to

evaluate in future work. The dissolution kinetics in Na_2SO_4 and in K_2CO_4 will be compared.

7.2.5 Other Surrogates

Ceria was used in this work as the surrogate for plutonium because of the identical oxidation state, crystal structure, thermodynamic properties and sintering behavior. Another metal oxide, hafnium oxide (HfO_2), has been reported as a surrogate for minor actinides (IV). [100] The reaction behavior of HfO_2 in the proposed reprocessing conditions will be studied.

LIST OF REFERENCES

[1] C. Degueldre, J.M. Paratte, J. Nucl. Mater. 274 (1999) 1-6.

[2] Y. W. Lee, C. Joung, S. Kim, S. C. Lee, Metals Mater. Inter. 7 (2001) 159-164.

[3] D. Bodansky, Physics Today, (2006) 80-81.

[4] M. Burghartz, H. Matzke, C. Léger, G. Vambenepe, M. Rome, J. Alloys Compd. 271-273 (1998) 544-548.

[5] H. Matzke, V.V. Rondinella, T. Wiss, J. Nucl. Mater. 274 (1999) 47-53.

[6] S. Bourg, F. Péron, J. Lacquement, J. Nucl. Mater. 360 (2007) 58-63.

[7] M.D.V. R.A. Verrall, V.D. Krstic, J. Nucl. Mater. 274 (1999) 54-60.

[8] J.F. K.H. Sarma, S-G. Lee, A.A. Solomon, J. Nucl. Mater. 352 (2006) 324–333

[9] N.S. Jacobson, E.J. Opila, D.L. Myers, E.H. Copland, J. Chem.Thermodynamics, 37 (2005) 1130-1137.

[10] M. Ichimura, E. Arai, P. Ramasamy, Jpn. J. Appl. Phys. 42 (2003) 4233-4236.

[11] D. Zhuang, J.H. Edgar, Mater. Sci. Eng.: R: Reports, 48 (2005) 1-46.

[12] A. Szczesny, P. Sniecikowski, J. Szmidt, A. Werbowy, Vacuum, 70 (2003) 249-254.

[13] M. Carruth, D. Baxter, F. Oliveira, K. Coley, J. Eur. Ceram. Soc. 18 (1998) 2331-2338.

[14] G.R. Pickrell, T. Sun, J.J. Brown, Fuel Proc. Tech. 44 (1995) 213-236.

[15] R. Naslain, Design, Compos. Sci. Tech. 64 (2004) 155-170.

[16] A.V. Zinovev, J.F. Moore, J. Hryn, M.J. Pellin, Surf. Sci. 600 (2006) 2242-2251.

[17] L. Pescayre, C. Passot, D. Cardonna, H. Chollet, J. Alloys Compd. 444-445 (2007) 603-605.

[18] F. Shojai, T.A. Mäntylä, Ceram. Inter. 27 (2001) 299-307.

[19] J.M. Perlado, J. Nucl. Mater. 251 (1997) 98-106.

[20] A.J.F. Rebelo, H.W. Scholz, H. Kolbe, G.P. Tartaglia, P. Fenici, J. Nucl. Mater. 258-263 (1998) 1582-1588.

[21] L.L. Snead, J.C. Hay, J. Nucl. Mater. 273 (1999) 213-220.

[22] A. Hasegawa, S. Nogami, T. Aizawa, K. Katou, K. Abe, J. Nucl. Mater. 307-311 (2002) 1152-1156.

[23] S.C.L. Y.W. Lee, H.S. Kim, C.Y. Joung, C. Degueldre, J. Nucl. Mater. 319 (2003) 15–23

[24] K.H. Park, T. Hinoki, A. Kohyama, J. Nucl. Mater. 367-370 (2007) 703-707.

[25] L.L. Snead, Y. Katoh, A. Kohyama, J.L. Bailey, N.L. Vaughn, R.A. Lowden, J. Nucl. Mater. 283-287 (2000) 551-555.

[26] Y. Katoh, H. Kishimoto, A. Kohyama, J. Nucl. Mater. 307-311 (2002) 1221-1226.

[27] G.A. Slack, J. Phys.Chem. Solids, 34 (1973) 321-335.

[28] W. Kowbel, C.A. Bruce, K.L. Tsou, K. Patel, J.C. Withers, G.E. Youngblood, J. Nucl. Mater. 283-287 (2000) 570-573.

[29] K.H. Park, Y. Katoh, H. Kishimoto, A. Kohyama, J. Nucl. Mater. 307-311 (2002) 1187-1190.

[30] T. Kawamura, D. Hori, Y. Kangawa, K. Kakimoto, M. Yoshimura, Y. Mori, Jpn. J. Appl. Phys. 47 (2008) 8898-8901.

[31] S. Kondo, K.H. Park, Y. Katoh, A. Kohyama, Fusion Sci. Tech. 44 (2003) 181-185.

[32] C.H. Henager Jr, A.L. Schemer-Kohrn, S.G. Pitman, D.J. Senor, K.J. Geelhood, C.L. Painter, J. Nucl. Mater. 378 (2008) 9-16.

[33] P.G. Medvedev, S.M. Frank, T.P. O'Holleran, M.K. Meyer, J. Nucl. Mater. 342 (2005) 48-62.

[34] E. Gomez, J. Echeberria, I. Iturriza, F. Castro, J. Eur. Ceram.Soc. 24 (2004) 2895-2903.

[35] S.G. Lee, J. Fourcade, R. Latta, A.A. Solomon, Fusion Eng. Design, 83 (2008) 713-719.

[36] P. Colombo, V. Sglavo, E. Pippel, J. Woltersdorf, J. Mater. Sci. 33 (1998) 2405-2412.

[37] S. Zhu, S. Ding, H.a. Xi, R. Wang, Mater. Letters, 59 (2005) 595-597.

[38] W.W. Pultz, J. Phys. Chem. 71 (1967) 4556-4558.

[39] J.A. Costello, R.E. Tressler, J. Am. Ceram. Soc. 69 (1986) 674-681.

[40] Z. Zheng, R.E. Tressler, K.E. Spear, J. Electrochem. Soc. 137 (1990) 2812-2816.

[41] T. Narushima, T. Goto, Y. Iguchi, T. Hirai, J. Am. Ceram. Soc. 74 (1991) 2583-2586.

[42] M. Balat, G. Flamant, G. Male, G. Pichelin, J. Mater. Sci. 27 (1992) 697-703.

[43] Y. Song, F.W. Smith, Appl. Phys. Lett. 81 (2002) 3061-3063.

[44] G.X. Wang, G.Q. Lu, B. Pei, A.B. Yu, J. Mater. Sc. 33 (1998) 1309-1317.

[45] H. Asteman, J.E. Svensson, M. Norell, L.G. Johansson, Oxid. Met. 54 (2000) 11-26.

[46] D.S. Fox, E.J. Opila, Q.N. Nguyen, D.L. Humphrey, S.M. Lewton, J. Am. Ceram. Soc. 86 (2003) 1256-1261.

[47] E.J. Opila, J. Am. Ceram. Soc. 86 (2003) 1238-1248.

[48] E.J. Opila, J. Am. Ceram. Soc. 82 (1999) 625-636.

[49] S. Shimada, T. Onuma, H. Kiyono, M. Desmaison, J. Am. Ceram. Soc. 89 (2006) 1218-1225.

[50] K.L. More, P.F. Tortorelli, M.K. Ferber, J.R. Keiser, J. Am. Ceram. Soc. 83 (2000) 211-213.

[51] E.J. Opila, R.E.H. Jr., J. Am. Ceram. Soc. 80 (1997) 197-205.

[52] C. Zhong, Y. Jiang, J. Gong, B. Deng, J. Li, Appl. Phys. A: Mater. Sci. Process. 97 (2009) 671-676.

[53] W.J. Lu, A.J. Steckl, T.P. Chow, W. Katz, J. Electrochem. Soc. 131 (1984) 1907-1914.

[54] A. Koh, A. Kestle, C. Wright, S.P. Wilks, P.A. Mawby, W.R. Bowen, Appl. Surf. Sci. 174 (2001) 210-216.

[55] E.J. Opila, Q.N. Nguyen, J. Am. Ceram. Soc. 81 (1998) 1949-1952.

[56] T. Goto, H. Homma, T. Hirai, Corros. Sci. 44 (2002) 359-370.

[57] T. Narushima, M. Kato, S. Murase, C. Ouchi, Y. Iguchi, J. Am. Ceram. Soc. 85 (2002) 2049-2055.

[58] C.K. Fink, J. Phys.: Condens. Matter, 21 (2009) 183001.

[59] R.E. Tressler, M.D. Meiser, T. Yonushonis, J. Am. Ceram. Soc. 59 (1976) 278 - 279.

[60] M. Azzi, J.J. Rameau, Corros. Sci. 24 (1984) 935-944.

[61] N.S. Jacobson, J. Am. Ceram. Soc. 69 (1986) 74-82.

[62] M. Azzi, J.J. Rameau, Corros. Sci. 30 (1990) 439-443, 445-449.

[63] J. Sha, J. Park, T. Hinoki, A. Kohyama, Mater. Trans. 46 (2005).

[64] S. Wu, L. Cheng, L. Zhang, Y. Xu, X. Luan, H. Mei, Compos. Part A: Appl. Sci. Manuf. 37 (2006) 1396-1401.

[65] A.R. Jones, R. Winter, G.N. Greaves, I.H. Smith, J. Phys. Chem. B, 109 (2005) 23154-23161

[66] M.D. Allendorf, K.E. Spearb, J. Electrochem. Soc.148 (2001) B59-B67.

[67] G. Liu, M. Li, Y. Zhou, Oxid. Metals, 66 (2006) 115-125.

[68] S.Y. Lee, Y.S. Park, P.P. Hsu, M.J. McNallan, J. Am. Ceram. Soc. 86 (2004) 1292-1298.

[69] I. Swiderski, W. Szczutowski, T. Niemyski, J. Crystal Growth, 21 (1974) 125-134.

[70] E.A. Burgemeister, W.v. Muench, E. Pettenpaul, J. Appl. Phys. 50 (1979) 5790-5795.

[71] N.K. Reddy, J. Mukerji, J. Am. Ceram. Soc. 74 (1991) 1139-1141.

[72] U. George, E. Rochau, H. Merk, J. Behnke, Germany patent, 1987.

[73] D.P. Dobson, A.P. Jones, R. Rabe, T. Sekine, K. Kurita, T. Taniguchi, T. Kondo, T. Kato, O. Shimomura, S. Urakawa, Earth Planet. Sci. Lett. 143 (1996) 207-215.

[74] J.H. Cameron, J. Pulp Paper Sci. 14 (1988) J76-J81.

[75] Y.I. Orlov, Glass Phys. .Chem. 28 (2002) 281-287.

[76] I. Odler, Special Inorganic Cements, 2000.

[77] A. Kosminski, D.P. Ross, J.B. Agnew, Fuel Process.Tech. 87 (2006) 1037-1049.

[78] M. Mohamedi, Y. Hisamitsu, I. Uchida, J. Appl. Electrochem. 32 (2002) 111-117.

[79] V.A. Volkovich, T.R. Griffiths, D.J. Fray, R.C. Thied, J. Nucl. Mater. 282 (2000) 152-158.

[80] R. Dimitrijevic, V. Dondur, J. Solid State Chem. 115 (1995) 214-224.

[81] G.S. Newth, A Text-Book Inorganic Chemistry, 6th ed., Longmans, 1898.

[82] J. Payá, J. Monzó, M.V. Borrachero, A. Mellado, L.M. Ordoñez, Cement Concr. Res. 31 (2001) 227-231.

[83] T. Cheng, R.H. Baney, J. Tulenko, J. Nucl. Mater. 405 (2010) 126-130.

[84] R.W. Reeve, A.C.C. Tseung, J. Electroanal. Chem. 403 (1996) 69-83.

[85] P. Tomczyk, M. Mosialek, Electrochim. Acta, 46 (2001) 3023-3032.

[86] S.H. White, U.M. Twardoch, The J. Electrochem. Soc. 134 (1987) 1080-1088

[87] G.J. Janz, J. Chem. Educ. 44 (1967) 581-590.

[88] H. Tanaka, J.Therm. Anal.Calorim. 32 (1987) 521-526.

[89] R.G.C. Beerkens, J. Am. Ceram. Soc. 84 (2001) 1952-1960.

[90] H.C. Yang, J. Korean Nucl.Soc. 34 (2002) 80-87.

[91] J.C. Marra, A.D. Cozzi, R.A. Pierce, J.M. Pareizs, A.R. Jurgensen, D.M. Missimer, Cerium as a surrogate in the plutonium immobilized form, Westinghouse Savannah River Company, (2002).

[92] Y.S. Park, H.Y. Sohn, D.P. Butt, J. Nucl. Mater. 280 (2000) 285-294.

[93] D.G. Kolman, Y. Park, M. Stan, R.J.H. Jr., D.P. Butt, An assessment of the validity of cerium oxide as a surrogate for plutonium oxide gallium removal studies, (1999) LA-UR-99-491.

[94] A.F. Wells, Structural Inorganic Chemistry, 5 ed., Clarendon Press, 1986.

[95] A.C. Tas, M. Akinc, J. Am. Ceram. Soc. 77 (1994) 2953-2960.

[96] H.A.M. van Hal, H.T. Hintzen, J. Alloys Compd. 179 (1992) 77-85.

[97] S. Zec, S. Boskovic, J. Nucl. Mater. 39 (2004) 5283-5286.

[98] R.L. Lehman, J.S. Gentry, N.G. Glumac, Thermochim. Acta. 316 (1998) 1-9.

[99] C. Shih, J. Tulenko, R. Baney, Mater. Res. Soc. Proc. 1215 (2010)

[100] C. Lopez, X. Deschanels, J.M. Bart, J.M. Boubals, C. Den Auwer, E. Simoni, J. Nucl. Mater. 312 (2003) 76-80.

BIOGRAPHICAL SKETCH

Ting Cheng was born on October, 1984 in Zhengzhou, China. She attended Wuhan University of Technology in 2002 and obtained her Bachelor of Engineering degree in Department of Materials Science and Engineering in 2006. During the four years in college, she joined in the projects of lead zirconate titanate (PZT)/epoxy composite fabrication and nano silver (Ag)/zinc oxide (ZnO_2) particle synthesis. The valuable research experience inspired her enthusiasm being a material scientist.

In 2006, she obtained an opportunity to pursuit advanced education at University of Florida. She started her first project on PZT/polyvinyl alcohol (PVA) nanofibers synthesis in Department of Materials Science and Engineering. In 2007, she joined Dr Baney's group to work on her doctoral project, reprocessing silicon carbide (SiC) inert matrix fuels. She also participated in the projects on exfoliating nanoclay and fabricating SiC at low temperature through collaboration with other group members. She received the degree of doctor of philosophy (Ph.D.) from the University of Florida in the fall of 2010. She will be married with Hao Zhang, her faithful life partner on January, 2011.